Dear Author,

Please, note that changes made to the HTML content will be added to the article before publication, but are not reflected in this PDF.

Note also that this file should not be used for submitting corrections.

Applied Mathematical Modelling xxx (2015) xxx–xxx

Contents lists available at ScienceDirect

Applied Mathematical Modelling

journal homepage: www.elsevier.com/locate/apm

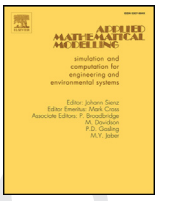

Semi-layerwise analysis of laminated plates with nonsingular delamination—The theorem of autocontinuity

Q1 András Szekrényes*

Budapest University of Technology and Economics Department of Applied Mechanics, Műegyetem rkp. 5, Building MM, Budapest 1111, Hungary

ARTICLE INFO

Article history:
Received 11 August 2014
Revised 19 May 2015
Accepted 26 June 2015
Available online xxx

Keywords:
Delamination
Mixed mode II/III fracture
Energy release rate
Third-order plate theory
Theoreom of autocontinuity

ABSTRACT

The proposed semi-layerwise approach captures the mechanical behavior of delaminated composite plates using four equivalent single layers independently of the lay-up. Two equivalent single layers are applied for both the top and bottom parts of a delaminated plate. The updated version of the system of exact kinematic conditions formulates the continuity of the in-plane displacements between the neighboring layers, the location of the global reference plane of the plate and – as important additions compared to previous papers – the continuity of shear strains, their derivatives and curvatures, respectively. The method is demonstrated using the first-, second- and third-order plate theories. As examples, simply supported delaminated plates are considered.The continuity between the delaminated and undelaminated plate regions is established through the theorem of autocontinuity. The J-integral is calculated along the straight delamination front and compared to the results of the virtual crack closure technique. The results indicate that the the first- and third-order plate theories provide the best solutions, and give good approximation even in those cases when the previous models failed, i.e., when the delamination is asymmetrically placed between two layers and it is close to the free surface of the plate.

© 2015 Published by Elsevier Inc.

UNCORRECTED PROOF

1. Introduction

Composite materials are susceptible to many type of damage modes [1–3]. One of them is delamination fracture induced by manufacturing and installation defects [4–8], low velocity impact [9–13], free edge effect [14,15] and the usage of notches and indentations [16,17] for the installation of the structure. The presence of cracks and delaminations in laminated composite beams and plates reduce significantly the stiffness and strength [18,19], moreover alter significantly the dynamical properties of the structure [20–25]. The stress intensity factor (SIF) [26–30] and energy release rate (ERR) [31–33] are the basic parameters of linear elastic fracture mechanics for the material characterization against delamination fracture (onset and propagation). The mode-I [34–43], mode-II [44–49], mode-III [50–63], and mixed-mode I/II [42,44,64–76], I/III [77,78], II/III [54,79–89], and I/II/III [90–92], fracture in composite materials is characterized by standard and nonstandard beam and plate specimens. While for beams the analytical solutions are relatively easy to develop, for plates similar exact solutions are difficult to obtain.

The classical (CLPT) or Kirchhoff [93–96], first-order (FSDT) [97–101], second-order (SSDT) [102,103,103–106], general third-order (TSDT) [107–111] and Reddy's [112–115] third-order shear deformation plate theories are widely-used in the composite

* Tel.: +36 14631170; fax: +36 14633471.
E-mail address: szeki@mm.bme.hu, szekrenyes.andras@gmail.com
URL: http://www.mm.bme.hu/~szeki

http://dx.doi.org/10.1016/j.apm.2015.06.037
S0307-904X(15)00453-9/© 2015 Published by Elsevier Inc.

Please cite this article as: A. Szekrényes, Semi-layerwise analysis of laminated plates with nonsingular delamination—The theorem of autocontinuity, Applied Mathematical Modelling (2015), http://dx.doi.org/10.1016/j.apm.2015.06.037

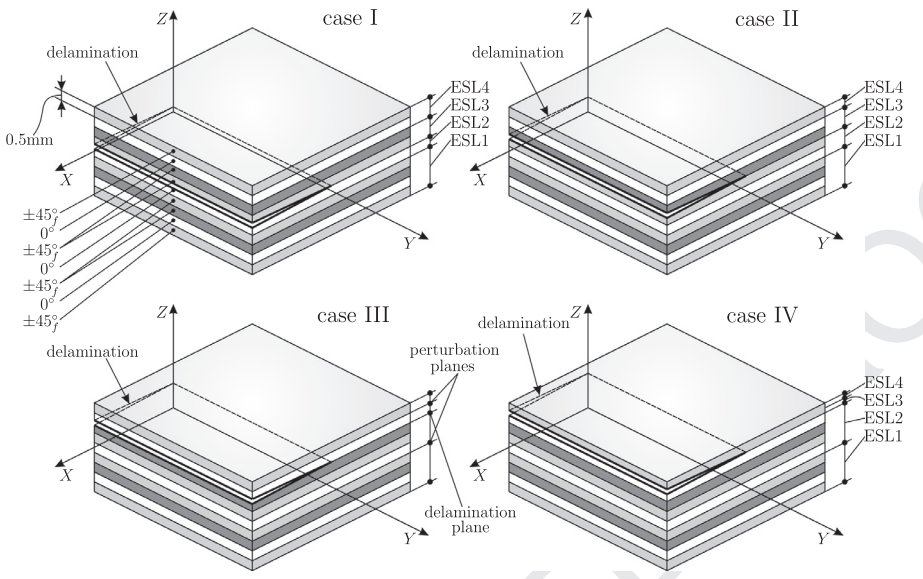

Fig. 1. Plate elements with orthotropic plies and the position of the delamination over the thickness of the plate.

literature to solve different plate problems in the field of statics, dynamics and stability. The layerwise (or zig-zag) theories [93,116–120] make it possible to calculate the interlaminar stresses more accurately than by using the ESL methods. However, the plate theories are applied only partially in the analysis of fracture mechanical tests, in most of the cases a 3D finite element (FE) analysis is preferred [121,122]. The finite element modeling of delaminations and cracks in 3D structures is computationally expensive. Typical examples in this respect are the different fracture mechanical configurations to determine the mode-III energy release rate [78,122].

Recently many articles were published on the modeling of the bending of composite plates with delamination using CLPT, FSDT, SSDT, TSDT for symmetrically [123–125] and asymmetrically [106,114,125,126] delaminated plates and by using layerwise approximations for in-plane loading and cylindrical bending [127–130]. The method of two ESLs was introduced in the former works and it was shown that for symmetric (midplane) delamination each method works well; however Reddy's third-order theory provides the best accuracy compared to FE results if the delamination is asymmetrically placed between two adjacent layers [114]. The mentioned problems involve typically mixed-mode II/III fracture conditions, in case it has already been shown that the coupling between the mode-II and mode-III SIFs could be significant [131,132].

This paper proposes the method of four ESLs for the delamination modeling of laminated composite plates. Three different theories are applied: FSDT, SSDT and general TSDT. The main aspect of the formulation is that the delamination plane divides the plate into a top and a bottom subplate. These subplates are modeled by two ESLs. The kinematic continuity is provided by the updated version of the system of exact kinematic conditions (SEKC) [114,125], the novelty is the specification of the continuity conditions with respect to the shear strain derivative and curvature. The displacement field satisfying the continuity conditions are formulated and the governing equations are derived based on variational calculus. Two simply-supported plates with delamination are examined and the Lévy plate formulation is used to reduce the system of PDEs to system of ODEs. The continuity between the delaminated and undelaminated portions has been formulated and it was highlighted that the number of constants in the solution functions is less than the number of continuity conditions. Therefore, in conjunction with the proposed 4ESL method the theorem of autocontinuity is introduced and a proof is given, as well. This theorem makes it possible to ensure the continuity between the delaminated and undelaminated portions by assigning the so-called autocontinuity parameters, which ensures the automatic continuity of first-, second- and third-order displacement terms in a reduced form. The displacement and stress fields in the laminated plates were determined by FSDT, SSDT and TSDT and at certain sections located in the delamination front were plotted along the thickness of the plate. The distributions of the J-integrals and mode mixities along the delamination front were also calculated and were compared to the results of the virtual crack closure technique (VCCT). The agreements and disagreements of the 2D analytical results with the numerical models are discussed.

2. Semi-layerwise laminated plate theory – the method of four ESLs

The concept of the semi-layerwise modeling is shown in Fig. 1. The plate elements contain an interfacial delamination, which divides the plate into a top and a bottom layer. Each layer is divided into further two ESLs. In other words the whole laminate is modeled by four ESLs – two above and below the delamination plane. The interface plane between two adjacent ESLs is the perturbation plane. The ESLs can be modeled by different plate theories. In this work the FSDT, SSDT and TSDT are applied to capture the mechanical fields. The components of the displacement field in general third-order plates can be written

Please cite this article as: A. Szekrényes, Semi-layerwise analysis of laminated plates with nonsingular delamination—The theorem of autocontinuity, Applied Mathematical Modelling (2015), http://dx.doi.org/10.1016/j.apm.2015.06.037

UNCORRECTED PROOF

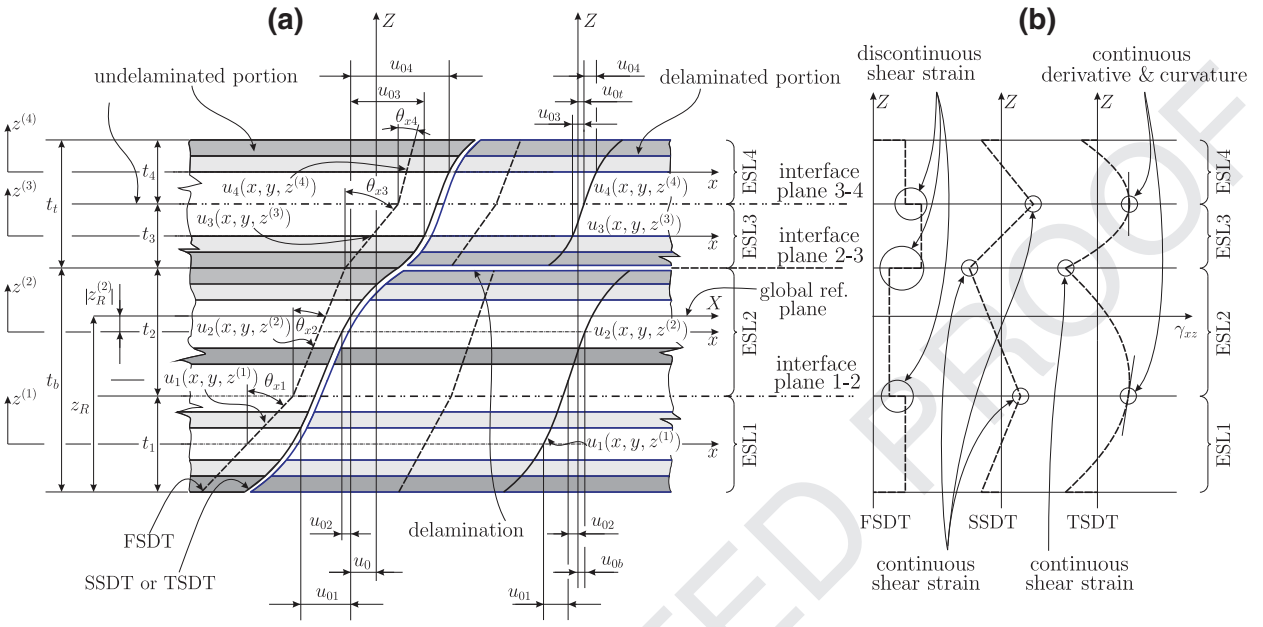

Fig. 2. Cross sections and deformation of the top and bottom plate elements of a delaminated plate in the *X*–*Z* plane (a). Distribution of the transverse shear strains by FSDT, SSDT and TSDT (b).

as [107–110]:

$$\begin{aligned} u_i(x,y,z^{(i)}) &= u_0(x,y) + u_{0i}(x,y) + \theta_{(x)i}(x,y)z^{(i)} + \phi_{(x)i}(x,y)(z^{(i)})^2 + \lambda_{(x)i}(x,y)(z^{(i)})^3 \\ v_i(x,y,z^{(i)}) &= v_0(x,y) + v_{0i}(x,y) + \theta_{(y)i}(x,y)z^{(i)} + \phi_{(y)i}(x,y)(z^{(i)})^2 + \lambda_{(y)i}(x,y)(z^{(i)})^3 \\ w_i(x,y) &= w_i(x,y), \end{aligned} \tag{1}$$

where i is the index of the actual ESL, $z^{(i)}$ is the local through thickness coordinate of the ith ESL, u_0 and v_0 are the global, u_{0i} and v_{0i} are the local membrane displacements; moreover, θ means the rotations of the cross sections about the X and Y axes (refer to Fig. 1), ϕ denotes the second-order, λ represents the third-order terms in the displacement functions. The displacement fields of FSDT and SSDT can be obtained by reducing Eq. (1) [98,133].

Definition (semi-layerwise plate model)**.** If a laminated plate with the N_l number of layers is modeled by the N_{ESL} number of equivalent single layers and $N_{ESL} < N_l$ then the model is called the semi-layerwise plate model. In this case the stiffness parameters and matrices of each ESL has to be determined based on the original lay-up of the plate. If $N_{ESL} = N_l$ then the model is a standard layerwise model.

3. The system of exact kinematic conditions – SEKC

The system of exact kinematic conditions has been formulated in [125] for first-order plates, later it was applied to second- [111] and third-order (Reddy) plates [114]. In the former papers the method of two ESLs was applied. Among the models published recently by the author it was shown that the best agreement with the VCCT results can be obtained by using the Reddy third-order theory. However, if the delamination is very close to the free surface of the plate then because of the perturbated stress state even Reddy's third-order theory predicts erroneously the shear stresses and the ERRs [114]. Therefore to perform some refinement the method of four ESLs is presented: both the top and bottom plates are captured by two ESLs.

In the sequel we treat only orthotropic composite plates containing an interfacial delamination between any two adjacent plies. The following formulation is valid in the general sense (with optional number of ESLs), as an illustration Figs. 2 and 3 show the concept in the *X*–*Z* and *Y*–*Z* planes of a plate with 4ESLs. The kinematic continuity of the field variables has to be established between each neighboring ESLs. First, the in-plane displacements have to be continuous at each interface (or perturbation) plane involving the following conditions:

$$(u_{(i)}, v_{(i)}, w_{(i)})|_{z^{(i)}=t_i/2} = (u_{(i+1)}, v_{(i+1)}, w_{(i+1)})|_{z^{(i+1)}=-t_{i+1}/2}, \tag{2}$$

where t denotes the thickness. If the global reference plane (given by $z_R^{(k)}$) is located in the kth layer, then at this plane the in-plane displacements are equal to the global membrane displacements u_0 and v_0 [93,94], viz.:

$$u_{(k)}|_{z^{(k)}=z_R^{(k)}} - u_0 = 0, v_{(k)}|_{z^{(k)}=z_R^{(k)}} - v_0 = 0. \tag{3}$$

Please cite this article as: A. Szekrényes, Semi-layerwise analysis of laminated plates with nonsingular delamination—The theorem of autocontinuity, Applied Mathematical Modelling (2015), http://dx.doi.org/10.1016/j.apm.2015.06.037

UNCORRECTED PROOF

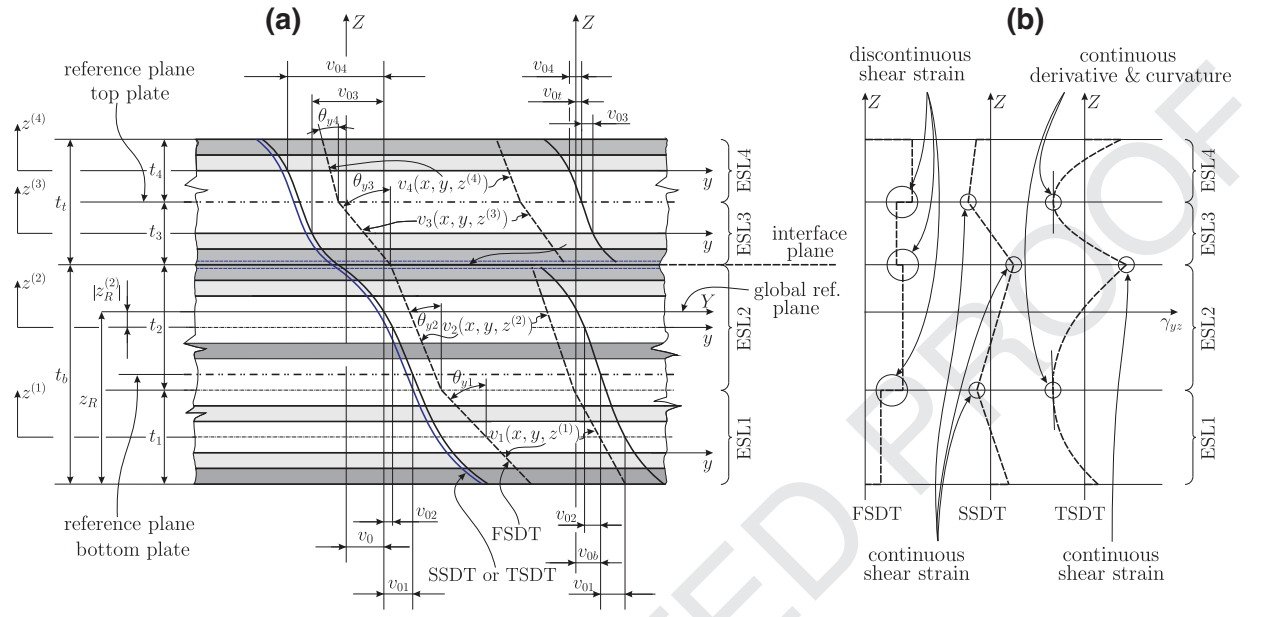

Fig. 3. Cross sections and deformation of the top and bottom plate elements of a delaminated plate in the *Y–Z* plane (a). Distribution of the transverse shear strains by FSDT, SSDT and TSDT (b).

The conditions given by Eqs. (2) and (3) are sufficient to develop semi-layerwise models using the FSDT. However, better accuracy can be achieved by using higher-order theories. If SSDT is applied then even the shear strains are assumed to be continuous across the interfaces:

$$(\gamma_{xz(i)}, \gamma_{yz(i)})|_{z^{(i)}=t_i/2} = (\gamma_{xz(i+1)}, \gamma_{yz(i+1)})|_{z^{(i+1)}=-t_{i+1}/2}. \tag{4}$$

It will be discussed later, that for third-order plates even the derivatives and the curvatures of the shear strains need to be continuous between the interfaces (otherwise the model becomes too compliant and leads to erroneous shear strain distributions):

$$\left(\frac{\partial \gamma_{xz(i)}}{\partial z^{(i)}}, \frac{\partial \gamma_{yz(i)}}{\partial z^{(i)}}\right)\Bigg|_{z^{(i)}=t_i/2} = \left(\frac{\partial \gamma_{xz(i+1)}}{\partial z^{(i+1)}}, \frac{\partial \gamma_{yz(i+1)}}{\partial z^{(i+1)}}\right)\Bigg|_{z^{(i+1)}=-t_{i+1}/2}, \tag{5}$$

and:

$$\left(\frac{\partial^2 \gamma_{xz(i)}}{\partial (z^{(i)})^2}, \frac{\partial^2 \gamma_{yz(i)}}{\partial (z^{(i)})^2}\right)\Bigg|_{z^{(i)}=t_i/2} = \left(\frac{\partial^2 \gamma_{xz(i+1)}}{\partial (z^{(i+1)})^2}, \frac{\partial^2 \gamma_{yz(i+1)}}{\partial (z^{(i+1)})^2}\right)\Bigg|_{z^{(i+1)}=-t_{i+1}/2}. \tag{6}$$

Based on the linear elasticity and assuming transversely inextensible deflection in each ESL, the SEKC formulates conditions using the in-plane displacement functions:

$$\frac{\partial^n (u_{(i)}, v_{(i)})}{\partial (z^{(i)})^n}, \quad n = 0, 1, 2, 3, \tag{7}$$

where $n = 0$ means condition against in-plane displacement, $n = 1$ means condition for shear strain, if $n = 2$ and $n = 3$ then a condition for the shear strain derivative and curvature is formulated.

4. Development of kinematically admissible displacement fields

In the sequel the SEKC is applied to the problem shown in Figs. 2 and 3. Therefore using the SEKC and the parameter elimination we modify the terms in Eq. (1).

Definition (Parameter elimination)**.** Certain parameters of the in-plane displacement functions can be eliminated using the SEKC requirements. The remaining (or *primary*) parameters are untouched, the parameters to be eliminated are the *secondary* parameters. The local membrane displacements and the second-order terms are typically secondary parameters, the global membrane displacements are primary parameters, the rotations and the third-order parameters are mixed (either primary or secondary) parameters. In the subsequent sections the undelaminated and delaminated regions are discussed separately. First, TSDT is considered and the SSDT and FSDT field equations are obtained by the reduction of TSDT model.

Please cite this article as: A. Szekrényes, Semi-layerwise analysis of laminated plates with nonsingular delamination—The theorem of autocontinuity, Applied Mathematical Modelling (2015), http://dx.doi.org/10.1016/j.apm.2015.06.037

UNCORRECTED PROOF

4.1. Undelaminated plate portion

Fig. 2a shows the transition zone around the delamination tip of the plate in the X–Z plate. The in-plane displacement distributions are linear in the case of FSDT, and curved if the SSDT or TSDT is applied. In Fig. 2b the corresponding shear strain distributions are shown: γ_{xz} is the piecewise constant if the FSDT is applied, piecewise linear if the fields are captured by SSDT and piecewise quadratic distribution can be obtained by TSDT. Fig. 3a and b show the same in the Y–Z plane. The in-plane displacement field has to satisfy the following conditions in accordance with Figs. 2a and 3a and the method of four ESLs:

$$\begin{aligned}(u_1, v_1, w_1)|_{z^{(1)}=t_1/2} &= (u_2, v_2, w_2)|_{z^{(2)}=-t_2/2},\\ (u_2, v_2, w_2)|_{z^{(2)}=t_2/2} &= (u_3, v_3, w_3)|_{z^{(3)}=-t_3/2},\\ (u_3, v_3, w_3)|_{z^{(3)}=t_3/2} &= (u_4, v_4, w_4)|_{z^{(4)}=-t_4/2}.\end{aligned} \tag{8}$$

The reference plane is located in the second ESL; therefore we have:

$$(u_2, v_2)|_{z^{(2)}=z_R^{(2)}} = (u_0(x,y), v_0(x,y)), \tag{9}$$

where based on figure $z_R^{(2)} = 1/2(t_3 + t_4 - t_1)$. The shear strains have to be continuous between the neighboring ESLs, i.e. we have:

$$\begin{aligned}(\gamma_{xz(1)}, \gamma_{yz(1)})|_{z^{(1)}=t_1/2} &= (\gamma_{xz(2)}, \gamma_{yz(2)})|_{z^{(2)}=-t_2/2},\\ (\gamma_{xz(2)}, \gamma_{yz(2)})|_{z^{(2)}=t_2/2} &= (\gamma_{xz(3)}, \gamma_{yz(3)})|_{z^{(3)}=-t_3/2},\\ (\gamma_{xz(3)}, \gamma_{yz(3)})|_{z^{(3)}=t_3/2} &= (\gamma_{xz(4)}, \gamma_{yz(4)})|_{z^{(4)}=-t_4/2}.\end{aligned} \tag{10}$$

To ensure the better distribution of the strains even the derivatives and the curvatures of the shear strains are imposed to be continuous at interface planes 1–2 and 3–4:

$$\begin{aligned}\left(\frac{\partial\gamma_{xz(1)}}{\partial z^{(1)}}, \frac{\partial\gamma_{yz(1)}}{\partial z^{(1)}}\right)\Bigg|_{z^{(1)}=t_1/2} &= \left(\frac{\partial\gamma_{xz(2)}}{\partial z^{(2)}}, \frac{\partial\gamma_{yz(2)}}{\partial z^{(2)}}\right)\Bigg|_{z^{(2)}=-t_2/2},\\ \left(\frac{\partial\gamma_{xz(3)}}{\partial z^{(3)}}, \frac{\partial\gamma_{yz(3)}}{\partial z^{(3)}}\right)\Bigg|_{z^{(3)}=t_3/2} &= \left(\frac{\partial\gamma_{xz(4)}}{\partial z^{(4)}}, \frac{\partial\gamma_{yz(4)}}{\partial z^{(4)}}\right)\Bigg|_{z^{(4)}=-t_4/2}.\end{aligned} \tag{11}$$

$$\begin{aligned}\left(\frac{\partial^2\gamma_{xz(1)}}{\partial (z^{(1)})^2}, \frac{\partial^2\gamma_{yz(1)}}{\partial (z^{(1)})^2}\right)\Bigg|_{z^{(1)}=t_1/2} &= \left(\frac{\partial^2\gamma_{xz(2)}}{\partial (z^{(2)})^2}, \frac{\partial^2\gamma_{yz(2)}}{\partial (z^{(2)})^2}\right)\Bigg|_{z^{(2)}=-t_2/2},\\ \left(\frac{\partial^2\gamma_{xz(3)}}{\partial (z^{(3)})^2}, \frac{\partial^2\gamma_{yz(3)}}{\partial (z^{(3)})^2}\right)\Bigg|_{z^{(3)}=t_3/2} &= \left(\frac{\partial^2\gamma_{xz(4)}}{\partial (z^{(4)})^2}, \frac{\partial^2\gamma_{yz(4)}}{\partial (z^{(4)})^2}\right)\Bigg|_{z^{(4)}=-t_4/2}.\end{aligned} \tag{12}$$

If Eq. (1) applies and the displacement functions are modified in order to satisfy Eqs. (8)–(12) then – using FSDT, SSDT or TSDT – it is possible to have:

$$\begin{aligned}u_i &= u_0 + \theta_{(x)i} z^{(i)} + \left(K_{ij}^{(0)} + K_{ij}^{(2)} (z^{(i)})^2 + K_{ij}^{(3)} (z^{(i)})^3\right)\psi_{(x)i},\\ v_i &= v_0 + \theta_{(y)i} z^{(i)} + \left(K_{ij}^{(0)} + K_{ij}^{(2)} (z^{(i)})^2 + K_{ij}^{(3)} (z^{(i)})^3\right)\psi_{(y)i}.\end{aligned} \tag{13}$$

where the matrices denoted by K_{ij} are related exclusively to the geometry; moreover $\boldsymbol{\psi}$ is the vector of primary parameters, finally $w_i(x,y) = w(x,y)$ for each ESLs, i.e. the transverse normals of each ESL are inextensible [93].

4.1.1. Third-order plate theory

Using the conditions above (Eqs. (8)–(12)) we can eliminate 22 parameters from Eq. (1), the secondary parameters are: u_{0i}, v_{0i}, $\phi_{(x)i}$, $\phi_{(y)i}$ for $i = 1..4$, $\lambda_{(x)i}$, $\lambda_{(y)i}$ for $i = 1, 2$ and 4. The primary parameters are: u_0, v_0, $\theta_{(x)i}$, $\theta_{(y)i}$ for $i = 1..4$ and $\lambda_{(x)3}$, $\lambda_{(y)3}$. The nonzero elements of the matrices $K_{ij}^{(0)}$, $K_{ij}^{(2)}$ and $K_{ij}^{(3)}$ are defined in Appendix A. The vector of primary parameters is: $\boldsymbol{\psi}_{(p)} = (\theta_{(p)1}\ \theta_{(p)2}\ \theta_{(p)3}\ \theta_{(p)4}\ \lambda_{(p)3})^T$ with $p = x$ or y.

4.1.2. Second-order plate theory

In this case $\lambda_{(x)i} = 0$ and $\lambda_{(y)i} = 0$ in Eq. (1). Eqs. (8) and (9) apply together with Eqs. (10) (shear strain continuity), however Eqs. (11) and (12) are omitted. Therefore we can eliminate 14 parameters from Eq. (1), the secondary parameters are: u_{0i}, v_{0i}, $\phi_{(x)i}$, $\phi_{(y)i}$ for $i = 1, 2$ and 4. The primary parameters are: u_0, v_0, $\theta_{(x)i}$, $\theta_{(y)i}$ for $i = 1..4$, $\phi_{(x)3}$ and $\phi_{(y)3}$. The nonzero elements of the matrices $K_{ij}^{(0)}$ and $K_{ij}^{(2)}$ are defined in Appendix B. Obviously $K_{ij}^{(3)} = 0$ in this case. The vector of primary parameters becomes: $\boldsymbol{\psi}_{(p)} = (\theta_{(p)1}\ \theta_{(p)2}\ \theta_{(p)3}\ \theta_{(p)4}\ \phi_{(p)3})^T$ with $p = x$ or y.

UNCORRECTED PROOF

Please cite this article as: A. Szekrényes, Semi-layerwise analysis of laminated plates with nonsingular delamination—The theorem of autocontinuity, Applied Mathematical Modelling (2015), http://dx.doi.org/10.1016/j.apm.2015.06.037

4.1.3. First-order plate theory

If the FSDT is applied then $\phi_{(x)i}=0$, $\phi_{(y)i}=0$, $\lambda_{(x)i}=0$ and $\lambda_{(y)i}=0$ in Eq. (1). Only Eq. (8) is utilized together with Eq. (9). The continuity of shear strains cannot be imposed. Thus we can eliminate eight parameters from Eq. (1), the secondary parameters are: u_{0i} and v_{0i} for $i=1..4$, The primary parameters are: u_0 and v_0 and $\theta_{(x)i}$, $\theta_{(y)i}$ for $i=1..4$. The nonzero elements of $K_{ij}^{(0)}$ are defined in Appendix C. $K_{ij}^{(2)}=0$ and $K_{ij}^{(3)}=0$ in this case. The vector of primary parameters is: $\boldsymbol{\psi}_{(p)}=(\theta_{(p)1}\ \theta_{(p)2}\ \theta_{(p)3}\ \theta_{(p)4})^T$ with $p=x$ or y.

4.2. Delaminated plate portion

In the delaminated portion (refer to Figs. 2 and 3) the top and bottom plates are modeled by two ESLs, and thus the first and third of Eq. (8) still hold. The definition of the top and bottom reference planes involve:

$$\begin{aligned}(u_1,v_1)|_{z^{(1)}=t_2/2}&=(u_{0b}(x,y),v_{0b}(x,y))\\(u_3,v_3)|_{z^{(3)}=t_4/2}&=(u_{0t}(x,y),v_{0t}(x,y))\end{aligned}\tag{14}$$

where u_{0b} and u_{0t} are the global membrane displacements of the bottom and top layers in accordance with Figs. 2 and 3. Moreover, the first and third of Eq. (10) apply again, as well as Eqs. (8) and (11) in the same form leading to ten conditions altogether.

4.2.1. Third-order plate theory

The first and third in Eq. (8) hold; moreover Eq. (14) is implied, again the first and third of Eq. (10) are utilized together with Eqs. (11) and (12) leading to 20 conditions altogether. The secondary parameters are: u_{0i}, v_{0i}, $\phi_{(x)i}$, $\phi_{(y)i}$ for $i=1..4$, $\lambda_{(x)i}$, $\lambda_{(y)i}$ for $i=2$ and 4. The primary parameters are: u_{0t}, v_{0t}, u_{0b}, v_{0b}, $\theta_{(x)i}$, $\theta_{(y)i}$ for $i=1..4$ and $\lambda_{(x)i}$, $\lambda_{(y)i}$ for $i=1$ and 3. The modified displacement field has the same form as that given by Eq. (13), the nonzero coefficients denoted by K are placed in Appendix A and: $\boldsymbol{\psi}_{(p)}=(\theta_{(p)1}\ \theta_{(p)2}\ \theta_{(p)3}\ \theta_{(p)4}\ \lambda_{(p)1}\ \lambda_{(p)3})^T$, where $p=x$ or y.

4.2.2. Second-order plate theory

In this case $\lambda_{(x)i}=0$ and $\lambda_{(y)i}=0$ in Eq. (1). The first and third in Eq. (8) hold; moreover Eq. (14) is implied, again the first and third of Eq. (10) is utilized; however Eqs. (11) and (12) are omitted. Therefore we can eliminate 12 parameters from Eq. (14), the secondary parameters are: u_{0i}, v_{0i} for $i=1..4$ and $\phi_{(x)i}$, $\phi_{(y)i}$ for $i=2$ and 4. The primary parameters are: u_{0t}, v_{0t}, u_{0b}, v_{0b}, $\theta_{(x)i}$, $\theta_{(y)i}$ for $i=1..4$, $\phi_{(x)i}$ and $\phi_{(y)i}$ for $i=2$ and 4. The nonzero elements of the matrices $K_{ij}^{(0)}$ and $K_{ij}^{(2)}$ are defined in Appendix B. Apparently $K_{ij}^{(3)}=0$ in this case. The vector of primary parameters takes the form: $\boldsymbol{\psi}_{(p)}=(\theta_{(p)1}\ \theta_{(p)2}\ \theta_{(p)3}\ \theta_{(p)4}\ \phi_{(p)1}\ \phi_{(p)3})^T$, where $p=x$ or y.

4.2.3. First-order plate theory

Similarly to the undelaminated portion we have: $\phi_{(x)i}=0$, $\phi_{(y)i}=0$, $\lambda_{(x)i}=0$ and $\lambda_{(y)i}=0$ in Eq. (1). Only the first and third of Eq. (8) apply together with Eq. (14). The shear strains are approximated by constant distributions in all four ESLs. Thus we can eliminate eight parameters from Eq. (1), the secondary parameters are: u_{0i} and v_{0i}, the primary parameters are: u_{0t}, v_{0t}, u_{0b}, v_{0b} and $\theta_{(x)i}$, $\theta_{(y)i}$ for $i=1..4$. The nonzero elements of $K_{ij}^{(0)}$ are defined in Appendix C. $K_{ij}^{(2)}=0$ $K_{ij}^{(3)}=0$ in this case and finally $\boldsymbol{\psi}_{(p)}=(\theta_{(p)1}\ \theta_{(p)2}\ \theta_{(p)3}\ \theta_{(p)4})^T$ with $p=x$ or y.

5. Equilibrium equations

If the displacement field is known, then the strain field is obtained by the following equation [134]:

$$\varepsilon_{ij}=\frac{1}{2}(u_{i,j}+u_{j,i}),\tag{15}$$

where ϵ_{ij} is the strain tensor, u_i is the displacement vector field. In plates assuming plane stress state the vector of in-plane strains is [93]:

$$\begin{Bmatrix}\varepsilon_x\\ \varepsilon_y\\ \gamma_{xy}\end{Bmatrix}_{(i)}=\begin{Bmatrix}\varepsilon_x^{(0)}\\ \varepsilon_y^{(0)}\\ \gamma_{xy}^{(0)}\end{Bmatrix}_{(i)}+z^{(i)}\cdot\begin{Bmatrix}\varepsilon_x^{(1)}\\ \varepsilon_y^{(1)}\\ \gamma_{xy}^{(1)}\end{Bmatrix}_{(i)}+[z^{(i)}]^2\cdot\begin{Bmatrix}\varepsilon_x^{(2)}\\ \varepsilon_y^{(2)}\\ \gamma_{xy}^{(2)}\end{Bmatrix}_{(i)}+[z^{(i)}]^3\cdot\begin{Bmatrix}\varepsilon_x^{(3)}\\ \varepsilon_y^{(3)}\\ \gamma_{xy}^{(3)}\end{Bmatrix}_{(i)}.\tag{16}$$

The vector of transverse shear strains becomes:

$$\begin{Bmatrix}\gamma_{xz}\\ \gamma_{yz}\end{Bmatrix}_{(i)}=\begin{Bmatrix}\gamma_{xz}^{(0)}\\ \gamma_{yz}^{(0)}\end{Bmatrix}_{(i)}+z^{(i)}\cdot\begin{Bmatrix}\gamma_{xz}^{(1)}\\ \gamma_{yz}^{(1)}\end{Bmatrix}_{(i)}+[z^{(i)}]^2\cdot\begin{Bmatrix}\gamma_{xz}^{(2)}\\ \gamma_{yz}^{(2)}\end{Bmatrix}_{(i)}\tag{17}$$

The stress field can be obtained by using the constitutive equation [93,94]. The stress resultants are calculated by integrating the stresses over the thicknesses of each ESL:

UNCORRECTED PROOF

Please cite this article as: A. Szekrényes, Semi-layerwise analysis of laminated plates with nonsingular delamination—The theorem of autocontinuity, Applied Mathematical Modelling (2015), http://dx.doi.org/10.1016/j.apm.2015.06.037

$$\begin{Bmatrix} N_{\alpha\beta} \\ M_{\alpha\beta} \\ L_{\alpha\beta} \\ P_{\alpha\beta} \end{Bmatrix}_{(i)} = \int_{-t_i/2}^{t_i/2} \sigma_{\alpha\beta} \begin{Bmatrix} 1 \\ z \\ z^2 \\ z^3 \end{Bmatrix}^{(i)} dz^{(i)}, \quad \begin{Bmatrix} Q_\alpha \\ R_\alpha \\ S_\alpha \end{Bmatrix}_{(i)} = \int_{-t_i/2}^{t_i/2} \sigma_{\alpha z} \begin{Bmatrix} 1 \\ z \\ z^2 \end{Bmatrix}^{(i)} dz^{(i)}, \tag{18}$$

where α and β takes x or y. The relationship between the strain field and the stress resultants can be written as:

$$\begin{Bmatrix} \{N\} \\ \{M\} \\ \{L\} \\ \{P\} \end{Bmatrix}_{(i)} = \begin{bmatrix} [A] & [B] & [D] & [E] \\ [B] & [D] & [E] & [F] \\ [D] & [E] & [F] & [G] \\ [E] & [F] & [G] & [H] \end{bmatrix}_{(i)} \begin{Bmatrix} \{\varepsilon^{(0)}\} \\ \{\varepsilon^{(1)}\} \\ \{\varepsilon^{(2)}\} \\ \{\varepsilon^{(3)}\} \end{Bmatrix}_{(i)}, \tag{19}$$

$$\begin{Bmatrix} \{Q\} \\ \{R\} \\ \{S\} \end{Bmatrix}_{(i)} = \begin{bmatrix} [A]^* & [B]^* & [D]^* \\ [B]^* & [D]^* & [E]^* \\ [D]^* & [E]^* & [F]^* \end{bmatrix}_{(i)} \begin{Bmatrix} \{\gamma^{(0)}\} \\ \{\gamma^{(1)}\} \\ \{\gamma^{(2)}\} \end{Bmatrix}_{(i)}, \tag{20}$$

where:

$$[..]^* = \begin{bmatrix} (.)_{55} & 0 \\ 0 & (.)_{44} \end{bmatrix}, \tag{21}$$

moreover: $\{N\}_{(i)}^{\mathrm{T}} = \{N_x\, N_y\, N_{xy}\}_{(i)}$ is the vector of in-plane forces, $\{M\}_{(i)}^{\mathrm{T}} = \{M_x\, M_y\, M_{xy}\}_{(i)}$ is the vector of bending and twisting moments, $\{Q\}_{(i)}^{\mathrm{T}} = \{Q_x\, Q_y\}_{(i)}$ is the vector of transverse shear forces, and finally $\{L\}_{(i)}^{\mathrm{T}} = \{L_x\, L_y\, L_{xy}\}_{(i)}$, $\{P\}_{(i)}^{\mathrm{T}} = \{P_x\, P_y\, P_{xy}\}_{(i)}$ and $\{R\}_{(i)}^{\mathrm{T}} = \{R_x\, R_y\}_{(i)}$, $\{S\}_{(i)}^{\mathrm{T}} = \{S_x\, S_y\}_{(i)}$ are the vectors of higher-order stress resultants. In Eq. (19) A_{ij} is the extensional, B_{ij} is coupling, D_{ij} is the bending, E_{ij}, F_{ij}, F_{ij} and H_{ij} are higher-order stiffnesses [114]:

$$(A_{ij}, B_{ij}, D_{ij}, E_{ij}, F_{ij}, G_{ij}, H_{ij})_{(i)} = \sum_{k=1}^{N_l} \int_{z_k}^{z_{k+1}} \bar{C}_{ij}^{(k)} (1, z, z^2, z^3, z^4, z^5, z^6)^{(i)} dz^{(i)}. \tag{22}$$

The stiffnesses above have to be calculated with respect to the local reference planes of each ESL. The equilibrium equations of the plate system can be obtained by using the virtual work principle [93]. In previous papers it was shown many times [114,125,126]. Therefore, here only the final results are given. To give the equilibrium equations in compact form we define the following vectors:

$$\begin{aligned} \mathbf{N}_i^{(x,xy)} &= (N_x \;\; N_{xy})_{(i)}^T, \quad \mathbf{N}_i^{(xy,y)} = (N_{xy} \;\; N_y)_{(i)}^T \\ \mathbf{M}_i^{(x,xy)} &= (M_x \;\; M_{xy})_{(i)}^T, \quad \mathbf{M}_i^{(xy,y)} = (M_{xy} \;\; M_y)_{(i)}^T \end{aligned} \tag{23}$$

Moreover, the vectors of higher-order stress resultants are:

$$\begin{aligned} \mathbf{L}_i^{(x,xy)} &= (L_x \;\; L_{xy})_{(i)}^T, \quad \mathbf{L}_i^{(xy,y)} = (L_{xy} \;\; L_y)_{(i)}^T \\ \mathbf{P}_i^{(x,xy)} &= (P_x \;\; P_{xy})_{(i)}^T, \quad \mathbf{P}_i^{(xy,y)} = (P_{xy} \;\; P_y)_{(i)}^T \end{aligned} \tag{24}$$

Finally the vectors of shear and higher-order forces become:

$$\mathbf{Q}_i = (Q_x \;\; Q_y)_{(i)}^T, \;\; \mathbf{R}_i = (R_x \;\; R_y)_{(i)}^T, \;\; \mathbf{S}_i = (S_x \;\; S_y)_{(i)}^T \tag{25}$$

In the sequel the equilibrium equations are derived separately for the undelaminated and delaminated parts.

5.1. Undelaminated portion

Formulating the total potential energy of the undelaminated plate portion based on the displacement field satisfying the SEKC requirements (Eq. (13)) the equilibrium equations can be obtained by variational calculus [93]. The equilibrium of the in-plane forces involves the following independently of the applied theory:

$$\delta u_0: \quad \sum_{i=1}^{4} \nabla \cdot \mathbf{N}_i^{(x,xy)} = 0, \;\; \delta v_0: \quad \sum_{i=1}^{4} \nabla \cdot \mathbf{N}_i^{(xy,x)} = 0, \tag{26}$$

where ∇ is the Hamilton differential operator [134]. In the general case (including FSDT, SSDT and TSDT) the number of primary parameters in the displacement field is k, the variation of the total potential energy results in the following equations:

$$\begin{aligned} \left.\begin{matrix} \delta\psi_{(x)k}: \\ \delta\psi_{(y)k}: \end{matrix}\right\} \quad & \sum_{i=1}^{4} K_{ik}^{(0)} \begin{pmatrix} \nabla \cdot \mathbf{N}_i^{(x,xy)} \\ \nabla \cdot \mathbf{N}_i^{(xy,y)} \end{pmatrix} + \alpha_{ik} \begin{pmatrix} \nabla \cdot \mathbf{M}_i^{(x,xy)} \\ \nabla \cdot \mathbf{M}_i^{(xy,y)} \end{pmatrix} + K_{ik}^{(2)} \begin{pmatrix} \nabla \cdot \mathbf{L}_i^{(x,xy)} \\ \nabla \cdot \mathbf{L}_i^{(xy,y)} \end{pmatrix} \\ & + K_{ik}^{(3)} \begin{pmatrix} \nabla \cdot \mathbf{P}_i^{(x,xy)} \\ \nabla \cdot \mathbf{P}_i^{(xy,y)} \end{pmatrix} + \beta_{ik} \begin{pmatrix} Q_{ix} \\ Q_{iy} \end{pmatrix} - 2K_{ik}^{(2)} \begin{pmatrix} R_{ix} \\ R_{iy} \end{pmatrix} - 3K_{ik}^{(3)} \begin{pmatrix} S_{ix} \\ S_{iy} \end{pmatrix} = 0, \end{aligned} \tag{27}$$

Please cite this article as: A. Szekrényes, Semi-layerwise analysis of laminated plates with nonsingular delamination—The theorem of autocontinuity, Applied Mathematical Modelling (2015), http://dx.doi.org/10.1016/j.apm.2015.06.037

UNCORRECTED PROOF

where $\psi_{(x)k}$ and $\psi_{(y)k}$ denote the primary parameters. Finally, the variation of the total potential energy with respect to the plate deflection provides:

$$\delta w: \sum_{i=1}^{4} \nabla \cdot \mathbf{Q}_i - q = 0, \tag{28}$$

and $q = q(x, y)$ is the function of external load [93]. As can be seen the differences among the equilibrium equations of FSDT, SSDT and TSDT are the matrices defined in Appendices A, B and C. Besides the matrices α_{ij} and β_{ij} are defined in the next section.

5.1.1. TSDT and SSDT

In the case of the TSDT and SSDT the matrices are defined as

$$\boldsymbol{\alpha} = -\boldsymbol{\beta} = \begin{pmatrix} 1 & 0 & 0 & 0 & 0 \\ 0 & 1 & 0 & 0 & 0 \\ 0 & 0 & 1 & 0 & 0 \\ 0 & 0 & 0 & 1 & 0 \end{pmatrix}. \tag{29}$$

5.1.2. FSDT

If the FSDT is applied then both $\boldsymbol{\alpha}$ and $\boldsymbol{\beta}$ is related to the Kronecker symbol: $\alpha_{ik} = -\beta_{ik} = \delta_{ik}$.

5.2. Delaminated portion

The delaminated region consist of a top and bottom plate. Each is modeled by two ESLs. Therefore, the global membrane displacements u_0, v_0 are replaced by u_{0b}, v_{0b} for ESL1 and ESL2, moreover by u_{0t}, v_{0t} for ESL3 and ESL4 in accordance with Figs. 2 and 3. Thus, the equilibrium equations of in-plane forces take the form below:

$$\begin{aligned} &\delta u_{0b}: \quad \sum_{i=1}^{2} \nabla \cdot \mathbf{N}_i^{(x,xy)} = 0, \quad \delta u_{0t}: \quad \sum_{i=3}^{4} \nabla \cdot \mathbf{N}_i^{(x,xy)} = 0, \\ &\delta v_{0b}: \quad \sum_{i=1}^{2} \nabla \cdot \mathbf{N}_i^{(xy,x)} = 0, \quad \delta v_{0t}: \quad \sum_{i=3}^{4} \nabla \cdot \mathbf{N}_i^{(xy,x)} = 0. \end{aligned} \tag{30}$$

The other equilibrium equations have the same form as those given by Eqs. (27) and (28).

5.2.1. TSDT and SSDT

If the TSDT and SSDT is used then the $\boldsymbol{\alpha}$ and $\boldsymbol{\beta}$ matrices become:

$$\boldsymbol{\alpha} = -\boldsymbol{\beta} = \begin{pmatrix} 1 & 0 & 0 & 0 & 0 & 0 \\ 0 & 1 & 0 & 0 & 0 & 0 \\ 0 & 0 & 1 & 0 & 0 & 0 \\ 0 & 0 & 0 & 1 & 0 & 0 \end{pmatrix}. \tag{31}$$

5.2.2. FSDT

If the FSDT is applied then $\alpha_{ik} = -\beta_{ik} = \delta_{ik}$. In the next section the solution of the equations is presented for simply-supported plates.

6. Examples – simply supported plates

The examples taken into account are simply supported laminated orthotropic plates with asymmetric delamination shown in Fig. 4a and b. The plates are loaded by a concentrated force. The same problem has been solved in previous papers [114,125,126] by using the method of two ESLs. In accordance with the Lévy plate formulation [135–136] the displacement parameters in Eqs. (13) are expressed by trial functions:

$$\begin{Bmatrix} \theta_x(x,y) \\ \theta_y(x,y) \\ \phi_x(x,y) \\ \phi_y(x,y) \\ \lambda_x(x,y) \\ \lambda_y(x,y) \end{Bmatrix} = \sum_{n=1}^{\infty} \begin{Bmatrix} X_n(x)\sin\beta y \\ Y_n(x)\cos\beta y \\ T_{xn}(x)\sin\beta y \\ T_{yn}(x)\cos\beta y \\ Z_{xn}(x)\sin\beta y \\ Z_{yn}(x)\cos\beta y \end{Bmatrix}, \quad \begin{Bmatrix} u_0(x,y) \\ v_0(x,y) \\ q(x,y) \\ w(x,y) \end{Bmatrix} = \sum_{n=1}^{\infty} \begin{Bmatrix} U_{0n}(x)\sin\beta y \\ V_{0n}(x)\cos\beta y \\ Q_n(x)\sin\beta y \\ W_n(x)\sin\beta y \end{Bmatrix}, \tag{32}$$

where $\beta = n\pi/b$. By taking back the solution in Eq. (32) into the equilibrium equations given by Eqs. (26)–(28) it is possible to reduce the system of PDEs to system of ODEs, which can be solved by the state-space formulation [138]. Even the stress

Please cite this article as: A. Szekrényes, Semi-layerwise analysis of laminated plates with nonsingular delamination—The theorem of autocontinuity, Applied Mathematical Modelling (2015), http://dx.doi.org/10.1016/j.apm.2015.06.037

UNCORRECTED PROOF

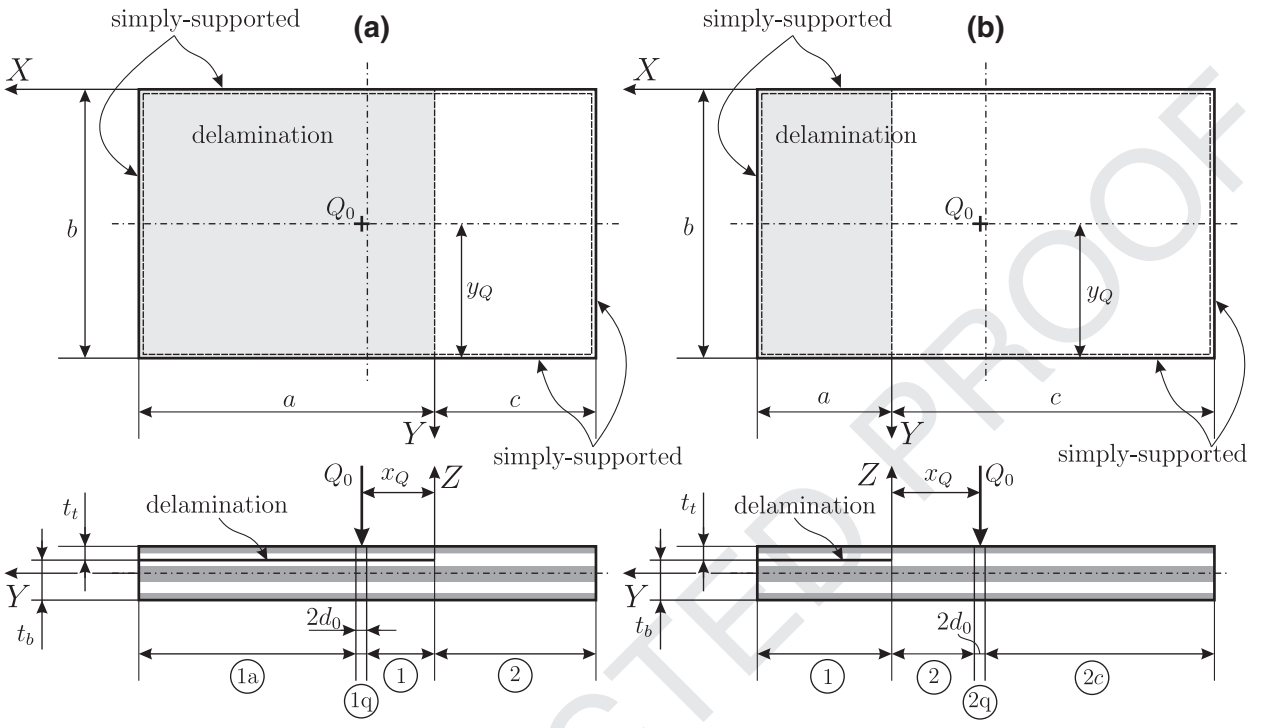

Fig. 4. Simply supported delaminated composite plates subjected to a concentrated force.

resultants can be expressed in terms of the displacement parameters through Eqs. (19) and (20). The state-space model takes the form [93,138]:

$$\mathbf{Z}' = \mathbf{T}\mathbf{Z} + \mathbf{F} \tag{33}$$

where $\mathbf{Z}$ is the state vector, $\mathbf{T}$ is the system matrix, and $\mathbf{F}$ is the vector of particular solutions. The general solution of Eq. (33) is:

$$\mathbf{Z}(x) = e^{\mathbf{T}x}\left(\mathbf{K} + \int_{x_0}^{x} e^{-\mathbf{T}\xi}\mathbf{F}(\xi)d\xi\right) = \mathbf{G}(x)\mathbf{K} + \mathbf{H}(x), \tag{34}$$

where $\mathbf{K}$ is the vector of constants. The parameters of the displacement field can be accessed by:

$$Z_i^{(d)} = \sum_{j=1}^{r} G_{ij}^{(d)} K_j^{(d)} + H_j^{(d)}, \quad Z_i^{(ud)} = \sum_{j=1}^{s} G_{ij}^{(ud)} K_j^{(ud)} + H_j^{(ud)}, \tag{35}$$

where subscript (d) refers to the delaminated (ud) means the undelaminated plate portion, r and s are the size of vectors, respectively. Since many papers have been published on the construction of the state-space model [104,111,114,124], the vectors and matrices in Eqs. (33)–(35) are discussed here only briefly.

6.1. Undelaminated region

In the case of the TSDT the state vector contains the parameters of vector $\boldsymbol{\psi}$ (refer to Sections 4.1.1, 4.1.2, 4.1.3), the global membrane parameters u_0 and v_0, the deflection w and the first derivatives of all these parameters leading to (and using the Lévy solution): $\mathbf{Z}^T = (U_{0n}, U'_{0n}, V_{0n}, V'_{0n}, [X_{in}, X'_{in}, Y_{in}, Y'_{in}], Z_{x3}, Z'_{x3}, Z_{y3}, Z'_{y3}, W_n, W'_n)$ for $i = 1..4$, i.e. the vector $\mathbf{Z}$ contains 26 elements, while the system matrix size is 26×26. If the SSDT is applied then Z_{x3} and Z_{y3} (and their derivatives) have to be replaced by T_{x3} and T_{y3} (refer to Eq. (32)), the size of the system vector and matrix is the same as that in the TSDT. Finally, the FSDT model involves only the membrane displacements, rotations and the deflection yielding a state vector with 22 elements and a system matrix with size of 22×22, respectively.

6.2. Delaminated region

The state vector of the TSDT model of the delaminated part contains the following elements $\mathbf{Z}^T = (U_{0bn}, U'_{0bn}, V_{0bn}, V'_{0bn}, U_{0tn}, U'_{0tn}, V_{0tn}, V'_{0tn}, [X_{in}, X'_{in}, Y_{in}, Y'_{in}], Z_{x1}, Z'_{x1}, Z_{y1}, Z'_{y1}, Z_{x3}, Z'_{x3}, Z_{y3}, Z'_{y3}, W_n, W'_n)$ for $i = 1..4$, i.e. the size of vector $\mathbf{Z}$ is 34, the system matrix size is 34×34. In the case of the SSDT Z_{xi} and Z_{yi}, $i = 1$ and 3 (and their derivatives) should be replaced by T_{xi} and T_{yi}, $i = 1$

Please cite this article as: A. Szekrényes, Semi-layerwise analysis of laminated plates with nonsingular delamination—The theorem of autocontinuity, Applied Mathematical Modelling (2015), http://dx.doi.org/10.1016/j.apm.2015.06.037

UNCORRECTED PROOF

and 3, the size of the state vector and system matrix is the same as that in the TSDT. The FSDT model involves the top and bottom membrane displacements, rotations and the deflection, consequently the state vector consists of 22 elements and system matrix size is 22×22, respectively.

In the next sections the boundary and continuity conditions are given for the TSDT model, the same for the SSDT and FSDT are placed in appendices.

7. Boundary conditions

The B.C.s of the problem in Fig. 4a at $x = a$ are determined through the displacement parameters:

$$(w, v_{0b}, v_{0t}, \theta_{y1}, \theta_{y2}, \theta_{y3}, \theta_{y4}, \lambda_{y1}, \lambda_{y3})^{(1a)}|_{x=a} = 0 \tag{36}$$

and the stress resultants:

$$(N_{x1} + N_{x2}, N_{x3} + N_{x4}, M_{x1}, M_{x2}, M_{x3}, M_{x4}, P_{x1}, P_{x3})^{(1a)}|_{x=a} = 0. \tag{37}$$

At $x = -c$ we have:

$$(w, v_0, \theta_{y1}, \theta_{y2}, \theta_{y3}, \theta_{y4}, \lambda_{y3})^{(2)}|_{x=-c} = 0, \tag{38}$$

$$(M_{x1}, M_{x2}, M_{x3}, P_{x3}, M_{x4}, N_{x1} + N_{x2} + N_{x3} + N_{x4})^{(2)}\big|_{x=-c} = 0. \tag{39}$$

8. Continuity conditions between regions (1) and (2)

The conditions between regions (1) and (2) (refer to Fig. 4a) involve the continuity of the displacement parameters and stress resultants. In the sequel, the continuity of the displacement field and stress resultants are discussed separately.

8.1. Continuity of stress resultants

To define the continuity conditions the equivalent stress resultants can be defined based on the equilibrium Eqs. (Eqs. (26) and (27)) and (30) and the vectors given by Eqs. (23) and (24):

$$\hat{\mathbf{M}}_i^{(x,xy)(1)} = \mathbf{M}_i^{(x,xy)(1)} + \sum_{j=1,4} \left(K_{ji}^{(0)} \mathbf{N}_j^{(x,xy)} + K_{ji}^{(2)} \mathbf{L}_j^{(x,xy)} \right)^{(1)}, \quad i = 1\ldots4, \tag{40}$$

$$\hat{\mathbf{P}}_3^{(x,y)(1)} = \sum_{i=3,4} \mathbf{P}_j^{(x,xy)(1)} + \sum_{j=3,4} \left(K_{j6}^{(0)} \mathbf{N}_j^{(x,xy)} + K_{j6}^{(2)} \mathbf{L}_j^{(x,xy)} \right)^{(1)}, \tag{41}$$

for the delaminated portion (1). Moreover, for the undelaminated region (2) we have:

$$\hat{\mathbf{M}}_i^{(x,xy)(2)} = \mathbf{M}_i^{(x,xy)(2)} + \sum_{j=1,4} \left(K_{ji}^{(0)} \mathbf{N}_j^{(x,xy)} + K_{ji}^{(2)} \mathbf{L}_j^{(x,xy)} + K_{ji}^{(3)} \mathbf{P}_j^{(x,xy)} \right)^{(2)}, \quad i = 1\ldots4, \tag{42}$$

$$\hat{\mathbf{P}}_3^{(x,y)(2)} = \sum_{i=1..4} \mathbf{P}_i^{(x,xy)(2)} + \sum_{j=1..4} \left(K_{j5}^{(0)} \mathbf{N}_j^{(x,xy)} + K_{j5}^{(2)} \mathbf{L}_j^{(x,xy)} \right)^{(2)}. \tag{43}$$

The continuity conditions using the equivalent stress resultants are:

$$\left(\hat{\mathbf{M}}_i^{(x,xy)}, \hat{\mathbf{P}}_3^{(x,y)}, \sum_{i=1..4} \mathbf{N}_i^{(x,xy)} \right)^{(1)}\Big|_{x=-0} = \left(\hat{\mathbf{M}}_i^{(x,xy)}, \hat{\mathbf{P}}_3^{(x,y)}, \sum_{i=1..4} \mathbf{N}_i^{(x,xy)(2)} \right)\Bigg|_{x=+0}, \quad i = 1\ldots4. \tag{44}$$

8.2. Continuity of displacement parameters

In the case of the general TSDT the continuity of the in-plane displacement is ensured only if the constant, linear, quadratic and cubic terms are exactly the same in the delamination front ($x = 0$). Because of the parameter elimination based on the SEKC it is not possible to match directly the constant, quadratic and cubic terms in the displacement function from layer by layer. Only the continuity of rotations can be defined between each ESL. In spite of that the continuity can be ensured indirectly (automatically) if certain conditions are met. The requirements of automatic continuity is formulated in the form of a theorem. We define the following set of parameters:

$$g_\alpha = (w, w', \theta_{x1}, \theta_{y1}, \theta_{x2}, \theta_{y2}, \theta_{x3}, \theta_{y3}, \theta_{x4}, \theta_{y4}\lambda_{x3}, \lambda_{y3}). \tag{45}$$

The continuity of the displacement parameters involves the following necessary conditions:

$$g_\alpha^{(1)}\Big|_{x=+0} = g_\alpha^{(2)}\Big|_{x=-0}. \tag{46}$$

However these are not sufficient. The sufficient conditions are presented through a theorem.

Please cite this article as: A. Szekrényes, Semi-layerwise analysis of laminated plates with nonsingular delamination—The theorem of autocontinuity, Applied Mathematical Modelling (2015), http://dx.doi.org/10.1016/j.apm.2015.06.037

UNCORRECTED PROOF

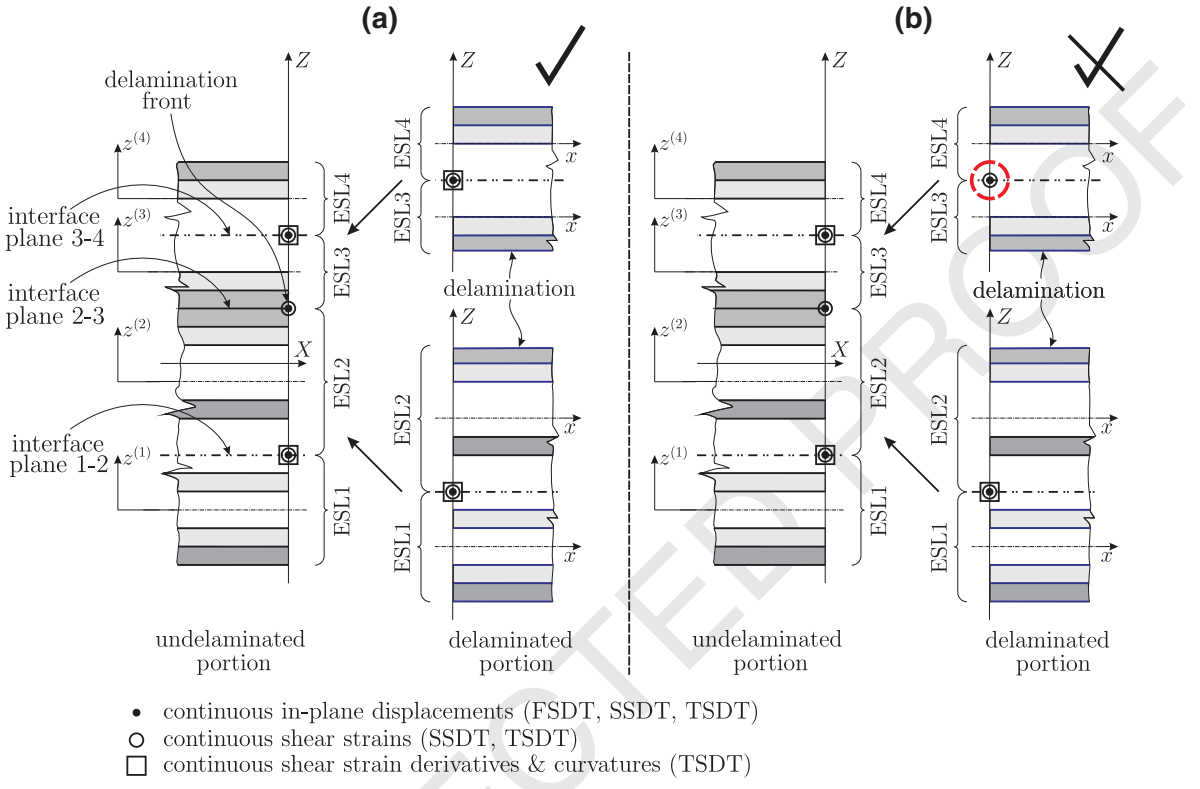

Fig. 5. Illustration of the theorem of autocontinuity: similar (a) and dissimilar (b) conditions are imposed at interface planes 1–2 and 3–4 of the delaminated and undelaminated parts.

248 *8.2.1. The theorem of autocontinuity (AC theorem)*

249 **Theorem.** *If the displacement field in the form of Eq. (13) in a laminated plate with delamination is developed by using the SEKC*
250 *requirements and $N_d \in \mathbb{N}$ and $N_{ud} \in \mathbb{N}$ are the numbers of eliminated parameters in the delaminated and undelaminated parts, respec-*
251 *tively, and $N_d \neq N_{ud}$, then the total continuity of the in-plane displacement functions of the delaminated and undelaminated plate parts*
252 *– apart from those imposed by Eq. (46) (mutual primary parameters) – can be ensured by imposing the continuity of $|N_d - N_{ud}| \in \mathbb{N}$*
253 *number of parameters. These parameters are the autocontinuity (or simply AC) parameters, which are at the same time primary pa-*
254 *rameters too. The autocontinuity is satisfied only if along interfaces 1–2 and 3–4 (Figs. 2 and 3) the same conditions are imposed in*
255 *the delaminated and undelaminated portions. Along the delamination plane (interface 2–3) different conditions can be applied. Fig. 5a*
256 *shows the case when the autocontinuity between the delaminated and undelaminated parts is satisfied, Fig. 5b indicates a case when*
257 *dissimilar conditions are imposed at interface 3–4 leading to discontinuous displacement field in the top plates.*

258 **Proof.** In the case of the TSDT model $N_d = 20$, $N_{ud} = 22$ (refer to Sections 4.1.1 and 4.2.1), so the number of AC parameters
259 is $|N_d - N_{ud}| = 2$. The AC parameters can be assigned based on the vector of primary parameters: the comparison of the $\boldsymbol{\psi}_{(p)}$
260 vectors in Sections 4.1.1 and 4.2.1 reveals that the AC parameters are λ_{x1} and λ_{y1} in the delaminated region. The comparison of
261 the displacement field (Eq. (13)) for the undelaminated and delaminated regions (Appendix A) reveals the following sufficient
262 conditions:

$$\lambda_{p1}\Big|^{(1)}_{x=+0} = \sum_{j=1..5} K^{(3)}_{3j}\psi_{(p)j}\Big|^{(2)}_{x=-0}, \quad p = x, y. \tag{47}$$

263 The former conditions ensure the continuity of the cubic terms in the displacement fields of regions (1) and (2) at $x = 0$
264 (Fig. 4a). Considering the fact that the parameters in g_β are continuous between regions (1) and (2) and by using the matrix
265 elements given in Appendix A it is possible to have the following expression for λ_{p1} at $x = +0$:

$$(\lambda_{p1})^{(1)}|_{x=+0} = \frac{4}{3}\left(\frac{1}{(t_1+t_2)}\left[\frac{\theta_{p1}}{(t_1+2t_2)} - \frac{\theta_{p2}}{t_2}\right] + \frac{(2t_3+t_4)\theta_{p3} - t_3\theta_{p4}}{t_2(t_3+t_4)(t_1+2t_2)}\right) + \frac{(2t_3+t_4)t_3\lambda_{p3}}{t_2(t_1+2t_2)}\Big|^{(2)}_{x=-0}. \tag{48}$$

Please cite this article as: A. Szekrényes, Semi-layerwise analysis of laminated plates with nonsingular delamination—The theorem of autocontinuity, Applied Mathematical Modelling (2015), http://dx.doi.org/10.1016/j.apm.2015.06.037

UNCORRECTED PROOF

Taking the former condition back into the quadratic part of the displacement field given by Eq. (13) of each ESL of the undelaminated part (2) yields the following at $x = -0$:

$$\sum_{j=1..5}\left(K^{(2)}_{1j}\psi^{*}_{(p)j}\right)\Big|^{(2)}_{x=-0} = \left(\frac{1}{(t_1+t_2)}\left[-\frac{(3t_2+2t_1)\theta_{p1}}{(t_1+2t_2)}+\frac{(t_1+2t_2)\theta_{p2}}{t_2}\right]-\frac{(2t_3+t_4)\theta_{p3}-t_3\theta_{p4}}{t_2(t_3+t_4)(t_1+2t_2)}\right) + \frac{(2t_3+t_4)t_3\lambda_{p3}}{t_2(t_1+2t_2)}\Big|^{(2)}_{x=-0}, \tag{49}$$

$$\sum_{j=1..5}\left(K^{(2)}_{2j}\psi^{*}_{(p)j}\right)\Big|^{(2)}_{x=-0} = \left(\frac{-1}{(t_1+t_2)}\left[\frac{t_2\theta_{p1}}{(t_1+2t_2)}+\frac{t_1\theta_{p2}}{t_2}\right] + \frac{(t_1+t_2)((2t_3+t_4)\theta_{p3}-t_3\theta_{p4})}{t_2(t_3+t_4)(t_1+2t_2)}\right)+\frac{3}{4}\frac{(2t_3+t_4)(t_1+t_2)t_3\lambda_{p3}}{t_2(t_1+2t_2)}\Big|^{(2)}_{x=-0}, \tag{50}$$

$$\sum_{j=1..5}\left(K^{(2)}_{3j}\psi^{*}_{(p)j}\right)\Big|^{(2)}_{x=-0} = \frac{-\theta_{p3}+\theta_{p4}}{(t_3+t_4)}-\frac{3}{4}(t_3+t_4)\lambda_{p3}\Big|^{(2)}_{x=-0}, \tag{51}$$

$$\sum_{j=1..5}\left(K^{(2)}_{4j}\psi^{*}_{(p)j}\right)\Big|^{(2)}_{x=-0} = \frac{-\theta_{p3}+\theta_{p4}}{(t_3+t_4)}+\frac{3}{4}(t_3+t_4)\lambda_{p3}\Big|^{(2)}_{x=-0}. \tag{52}$$

Simultaneously, by taking back Eq. (48) into the displacement functions of every ESL of the delaminated part (1) defined by Eq. (13) we have at $x = +0$:

$$\sum_{j=1..6}\left(K^{(2)}_{1j}\psi^{*}_{(p)j}\right)\Big|^{(1)}_{x=+0} = \left(\frac{1}{(t_1+t_2)}\left[-\frac{(3t_2+2t_1)\theta_{p1}}{(t_1+2t_2)}+\frac{(t_1+2t_2)\theta_{p2}}{t_2}\right] - \frac{(2t_3+t_4)\theta_{p3}-t_3\theta_{p4}}{t_2(t_3+t_4)(t_1+2t_2)}\right)+\frac{(2t_3+t_4)t_3\lambda_{p3}}{t_2(t_1+2t_2)}\Big|^{(1)}_{x=+0}, \tag{53}$$

$$\sum_{j=1..6}\left(K^{(2)}_{2j}\psi^{*}_{(p)j}\right)\Big|^{(1)}_{x=+0} = \left(\frac{-1}{(t_1+t_2)}\left[\frac{t_2\theta_{p1}}{(t_1+2t_2)}+\frac{t_1\theta_{p2}}{t_2}\right] + \frac{(t_1+t_2)((2t_3+t_4)\theta_{p3}-t_3\theta_{p4})}{t_2(t_3+t_4)(t_1+2t_2)}\right)+\frac{3}{4}\frac{(2t_3+t_4)(t_1+t_2)t_3\lambda_{p3}}{t_2(t_1+2t_2)}\Big|^{(1)}_{x=+0}, \tag{54}$$

$$\sum_{j=1..6}\left(K^{(2)}_{3j}\psi^{*}_{(p)j}\right)\Big|^{(1)}_{x=-0} = \frac{-\theta_{p3}+\theta_{p4}}{(t_3+t_4)}-\frac{3}{4}(t_3+t_4)\lambda_{p3}\Big|^{(1)}_{x=-0}, \tag{55}$$

$$\sum_{j=1..6}\left(K^{(2)}_{4j}\psi^{*}_{(p)j}\right)\Big|^{(1)}_{x=+0} = \frac{-\theta_{p3}+\theta_{p4}}{(t_3+t_4)}+\frac{3}{4}(t_3+t_4)\lambda_{p3}\Big|^{(1)}_{x=+0}. \tag{56}$$

Obviously, the right-hand sides of Eqs. (49)–(52) and Eqs. (53)–(56) are the same. Considering the continuity of the parameters in Eq. (45) by Eq. (46) it can be seen that the continuity of the quadratic term in the displacement functions of regions (1) and (2) is automatically satisfied. □

Consequence. If the continuity of linear terms (rotations) in the displacement field in each ESL given by Eq. (13) are continuous, moreover the continuity of quadratic and cubic terms of each ESL are imposed using the AC parameters, then the continuity of the membrane displacement components between the top plates (as well as the bottom plates) of the delaminated and undelaminated regions can be ensured by imposing the equality between the membrane (constant) displacement terms of only a single ESL in the delaminated part and a single one in the undelaminated part, but not in every ESLs. The ESLs can be chosen optionally, however the chosen ESLs should be in the same through-thickness position in the delaminated and undelaminated

UNCORRECTED PROOF

Please cite this article as: A. Szekrényes, Semi-layerwise analysis of laminated plates with nonsingular delamination—The theorem of autocontinuity, Applied Mathematical Modelling (2015), http://dx.doi.org/10.1016/j.apm.2015.06.037

plate regions. In this case the continuity of the membrane parts in the other ESLs is satisfied automatically. We choose the first (in the bottom layer) and third (in top layer) ESLs to impose the continuity of the membrane displacements using the equations below:

$$\begin{pmatrix} u_{0b} \\ v_{0b} \end{pmatrix} + \sum_{j=1,2,5} K_{1j}^{(0)} \begin{pmatrix} \psi_{(x)j} \\ \psi_{(y)j} \end{pmatrix} \Bigg|_{x=+0}^{(1)} = \begin{pmatrix} u_0 \\ v_0 \end{pmatrix} + \sum_{j=1..5} K_{1j}^{(0)} \begin{pmatrix} \psi_{(x)j} \\ \psi_{(y)j} \end{pmatrix} \Bigg|_{x=-0}^{(2)},$$
$$\begin{pmatrix} u_{0t} \\ v_{0t} \end{pmatrix} + \sum_{j=3,4,6} K_{3j}^{(0)} \begin{pmatrix} \psi_{(x)j} \\ \psi_{(y)j} \end{pmatrix} \Bigg|_{x=+0}^{(1)} = \begin{pmatrix} u_0 \\ v_0 \end{pmatrix} + \sum_{j=1..5} K_{3j}^{(0)} \begin{pmatrix} \psi_{(x)j} \\ \psi_{(y)j} \end{pmatrix} \Bigg|_{x=-0}^{(2)}. \tag{57}$$

9. Continuity between regions (1)–(1q) and (1q)–(1a)

The continuity between regions (1)–(1q) and (1q)–(1a) (see Fig. 4a) can be imposed by defining the sets of parameters below:

$$g_\beta = (u_{0b}, u_{0t}, v_{0b}, v_{0t}, w, w', \theta_{xi}, \theta_{yi}, \lambda_{x1}, \lambda_{y1}, \lambda_{x3}, \lambda_{y3}), \quad i = 1\ldots4, \tag{58}$$

$$g_\gamma = \left(\hat{M}_{xi}, P_{x1}, P_{x3}, \sum_{i=1..2} N_{xi}, \sum_{i=3..4} N_{xi}, \hat{M}_{xyi}, P_{xy1}, P_{xy3}, \sum_{i=1..2} N_{xyi}, \sum_{i=3..4} N_{xyi} \right), \quad i = 1\ldots4. \tag{59}$$

The continuity conditions are (refer to Fig. 4a):

$$g_\beta^{(1)}\Big|_{x=x_0-d_0} = g_\beta^{(1q)}\Big|_{x=x_0-d_0}, \quad g_\gamma^{(1)}\Big|_{x=x_0-d_0} = g_\gamma^{(1q)}\Big|_{x=x_0-d_0}, \tag{60}$$

$$g_\beta^{(1q)}\Big|_{x=x_0+d_0} = g_\beta^{(1a)}\Big|_{x=x_0+d_0}, \quad g_\gamma^{(1q)}\Big|_{x=x_0+d_0} = g_\gamma^{(1a)}\Big|_{x=x_0+d_0}. \tag{61}$$

The summary of the equations results in: Eq. (36)–(39) means 30 B.C.s, Eqs. (44), (46), (47) and (57) yields 30 conditions between regions (1) and (2). Eqs. (60) and (61) provides 2 × 34 conditions. That means 30 + 30 + 34 + 34 = 128 conditions altogether in the case of the TSDT solution of problem a in Fig. 4. Problem b in Fig. 4 can be solved similarly; therefore the details are not given. The B.C.s and the C.C.s for the FSDT and SSDT models can be defined similarly, these are discussed in Appendix D.

In the sequel through some definitions it is explained why the dynamic boundary conditions [114] are not imposed at the traction-free surfaces of the plate.

Definition (Over-constrained plate model)**.** If the displacement field given by Eq. (13) is developed by using the SEKC requirements and the resulting equilibrium equations by the basic theory of elasticity, as well as the solution of the corresponding boundary value problem do not make it possible to provide the continuity of the equivalent bending ($\hat{M}_x$) and twisting moments ($\hat{M}_{xy}$), between each ESL, moreover the sum of in-plane normal (N_x) and shear forces (N_{xy}) of the delaminated and undelaminated plate regions, then the model becomes over-constrained. The result of the over-constraining is the bad estimation of the displacement, strain and stress fields.

Definition (Well-constrained plate model)**.** If the solution of the boundary value problem (the number of constants in the solutions functions) makes it possible to provide the continuity of the of the equivalent bending ($\hat{M}_x$) and twisting moments ($\hat{M}_{xy}$) between each ESL, moreover the sum of in-plane normal (N_x) and shear forces (N_{xy}) of the delaminated and undelaminated plate regions, then the model is well-constrained.

The models proposed in this paper are well-constrained models. If we impose even the dynamic BC.s [114], then in the delaminated portion there are four traction-free surfaces, leading to eight further conditions. Moreover in the undelaminated part, there are two traction-free surfaces involving four dynamic B.C.s. Due to these conditions the number of parameters that should be eliminated from Eq. (13) leads to an over-constrained model with incorrect results, although the autocontinuity is satisfied even in this case.

10. J-integral

The J-integral for FSDT, SSDT and TSDT has already been derived for plates with symmetric [104,111,123,124] and asymmetric [114,125,126] lay-up. Therefore, in this work the details are not discussed. The mode-II and mode-III J-integrals are given in Appendix E.

Please cite this article as: A. Szekrényes, Semi-layerwise analysis of laminated plates with nonsingular delamination—The theorem of autocontinuity, Applied Mathematical Modelling (2015), http://dx.doi.org/10.1016/j.apm.2015.06.037

UNCORRECTED PROOF

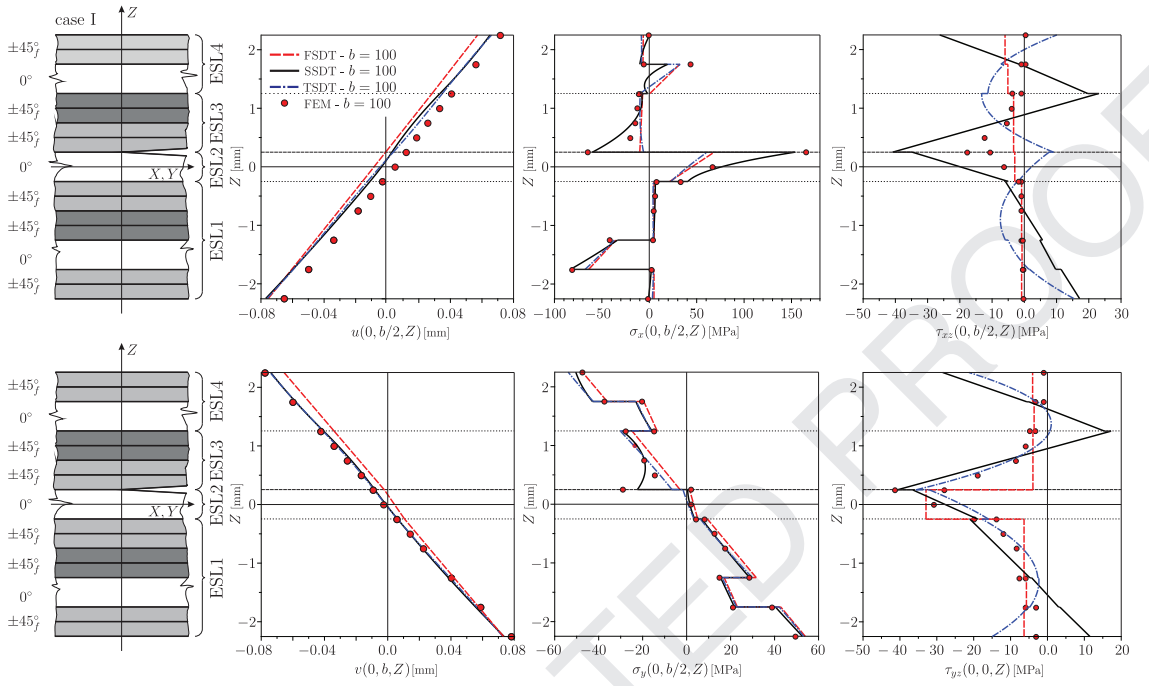

Fig. 6. Distribution of the in-plane displacements (u and v), normal stresses (σ_x and σ_y) and shear stresses (τ_{xz} and τ_{yz}) over the plate thickness for example in Fig. 4a, case I, $b = 100$ mm.

11. Results and discussions

To demonstrate the accuracy of the analytical models two examples shown in Fig. 4 are solved. The data of the problem depicted in Fig. 4a are: $a = 105$ mm (delamination length), $c = 55$ mm (undelaminated length), $b = 100$ and $b = 160$ mm (plate width), $t_t + t_b = 4.5$ mm (plate thickness), $Q_0 = 1000$ N, $x_Q = 31$ mm, $y_Q = 50$ mm and $y_Q = 80$ mm (point of action coordinates of Q_0), $d_0 = 0.1$ mm. For the problem in Fig. 4b the data are: $a = 55$ mm (delamination length), $c = 35$ mm (undelaminated length), $b = 60$ and $b = 90$ mm (plate width), $t_t + t_b = 4.5$ mm (plate thickness), $Q_0 = 10000$ N, $x_Q = 11$ mm, $y_Q = 30$ mm and $y_Q = 45$ mm (point of action coordinates of Q_0), $d_0 = 0.1$ mm. The material of the plates is carbon/epoxy. The lay-up of the plate is $[\pm 45^f/0/\pm 45^f_2/\bar{0}]_S$, the material properties can be found in [114]. Finite element models were also constructed to validate the analytical results. The details of the FE models are presented in a recent paper [114]. The position of the delamination was varied in the through thickness direction, these were assigned as cases I, II, III and IV in accordance with Fig. 1, respectively.

11.1. Displacement and stress distributions

Fig. 6 shows the distribution of the in-plane displacements u and v, normal stresses σ_x, σ_y and shear stresses τ_{xz} and τ_{yz} in specified cross sections at the delamination front for case I, when the delamination is near the midplane. The results of the FSDT, SSDT, TSDT and FE solutions are presented. The displacement curves show very moderate nonlinearity, it can be seen that considering both components the TSDT provides the best fit to the numerical results. In contrast it is the SSDT that approximates the normal stresses (σ_x and σ_y) in the best way, especially the peak in the plane of the delamination. Regarding the shear stresses the TSDT provides the highest accuracy compared to the FE results. In the case of the SSDT it is clear that the model becomes overperturbated, i.e. large fluctuations take place in the through thickness distribution of τ_{xz} and τ_{yz}. In the case of the shear stresses, each theory approximates well the area under the distribution by FEM.

The distributions of case II are presented in Fig. 7. Again, the TSDT provides the best fit to the displacement distributions by FEM. However, this time it is FSDT that fits the normal stresses in the best way. The TSDT and FSDT approximate the shear stresses well, the SSDT result becomes again overperturbated. The reason for the large fluctuations in the distribution are the uncontrolled derivatives (Eq. (5)) of the displacement functions.

Cases III and IV – when the delamination is located closer to the top surface of the plate – are demonstrated through Figs. 8 and 9. Briefly summarizing the results, it can be seen that SSDT provides inaccurate predictions for the shear stresses, it is clear that this model should be abandoned. On the contrary the FSDT and TSDT are still very reasonable to approximate the mechanical fields. The most accurate results are obtained by the TSDT model.

UNCORRECTED PROOF

Please cite this article as: A. Szekrényes, Semi-layerwise analysis of laminated plates with nonsingular delamination—The theorem of autocontinuity, Applied Mathematical Modelling (2015), http://dx.doi.org/10.1016/j.apm.2015.06.037

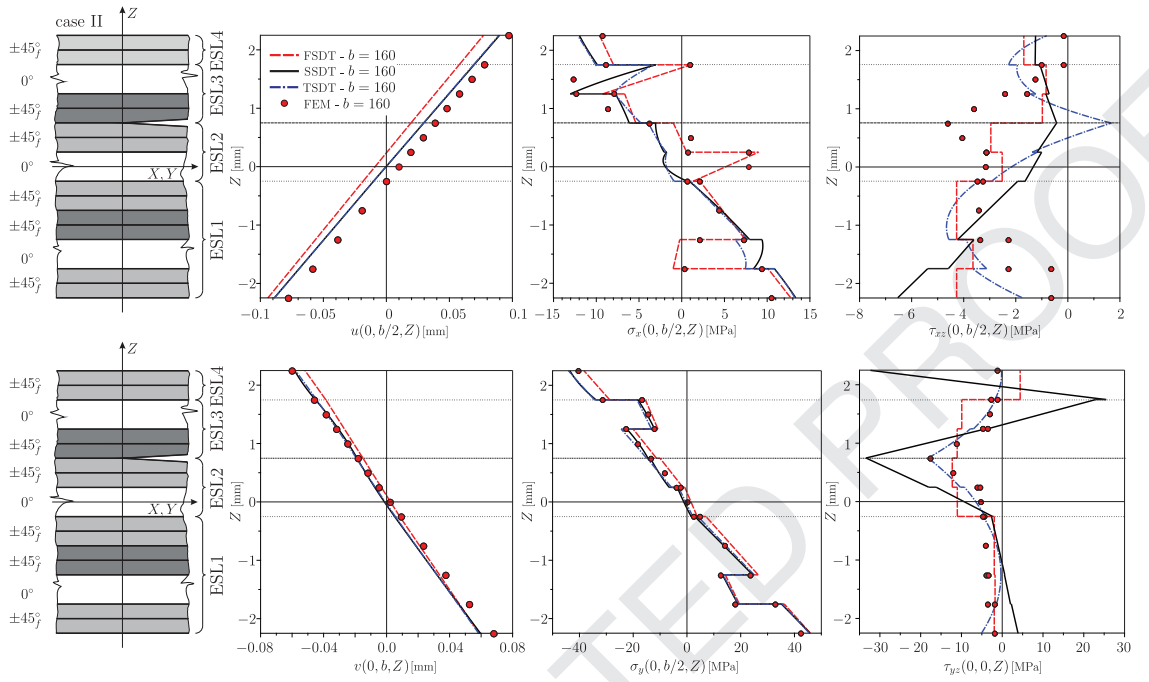

Fig. 7. Distribution of the in-plane displacements (u and v), normal stresses (σ_x and σ_y) and shear stresses (τ_{xz} and τ_{yz}) over the plate thickness for example in Fig. 4a, case II, $b = 160$ mm.

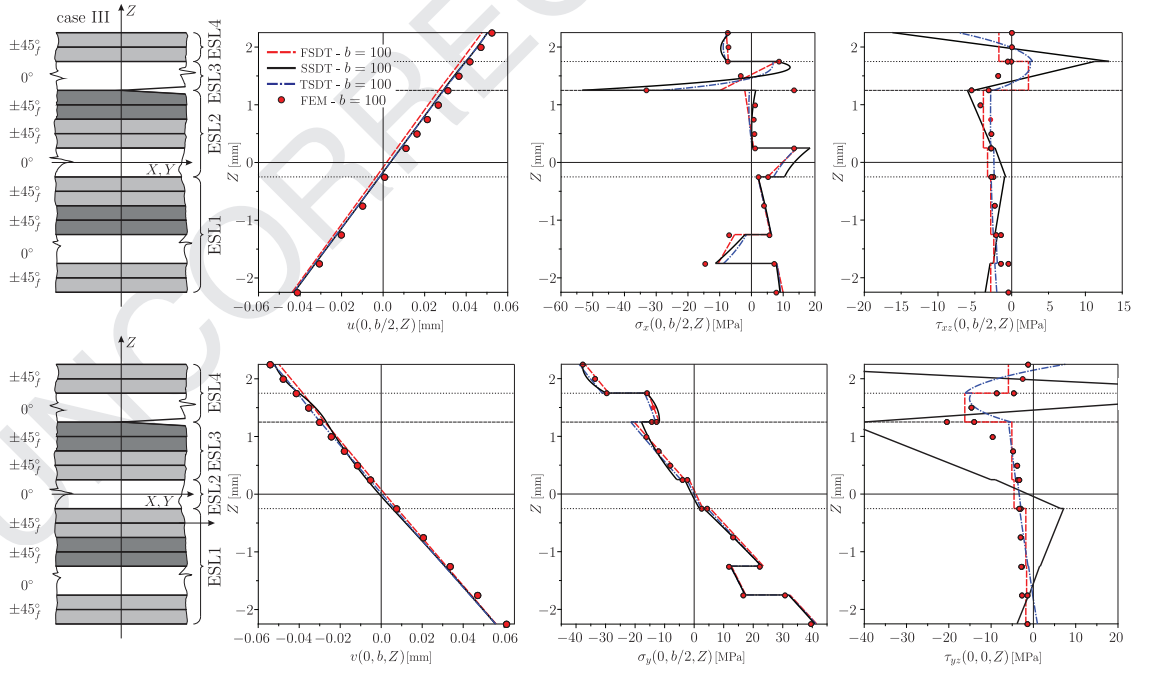

Fig. 8. Distribution of the in-plane displacements (u and v), normal stresses (σ_x and σ_y) and shear stresses (τ_{xz} and τ_{yz}) over the plate thickness for example in Fig. 4a, case III, $b = 100$ mm.

The results of problem b in Fig. 4 are plotted in Figs. 10–13. It is shown that in this example because of the smaller plate dimensions and the shorter crack length the perturbation in the mechanical fields is significantly more intense than in problem a. Case I is displayed in Fig. 10. An immediate observation is that u displacement by FEM is inaccurately predicted by all of the theories. Nevertheless, it has to be emphasized that the load of problem b is Q_0=10000 N, i.e. ten times higher than that of problem a. Thus, smaller displacements and – as Fig. 10 shows – significantly higher stresses are obtained. In case I the normal

Please cite this article as: A. Szekrényes, Semi-layerwise analysis of laminated plates with nonsingular delamination—The theorem of autocontinuity, Applied Mathematical Modelling (2015), http://dx.doi.org/10.1016/j.apm.2015.06.037

UNCORRECTED PROOF

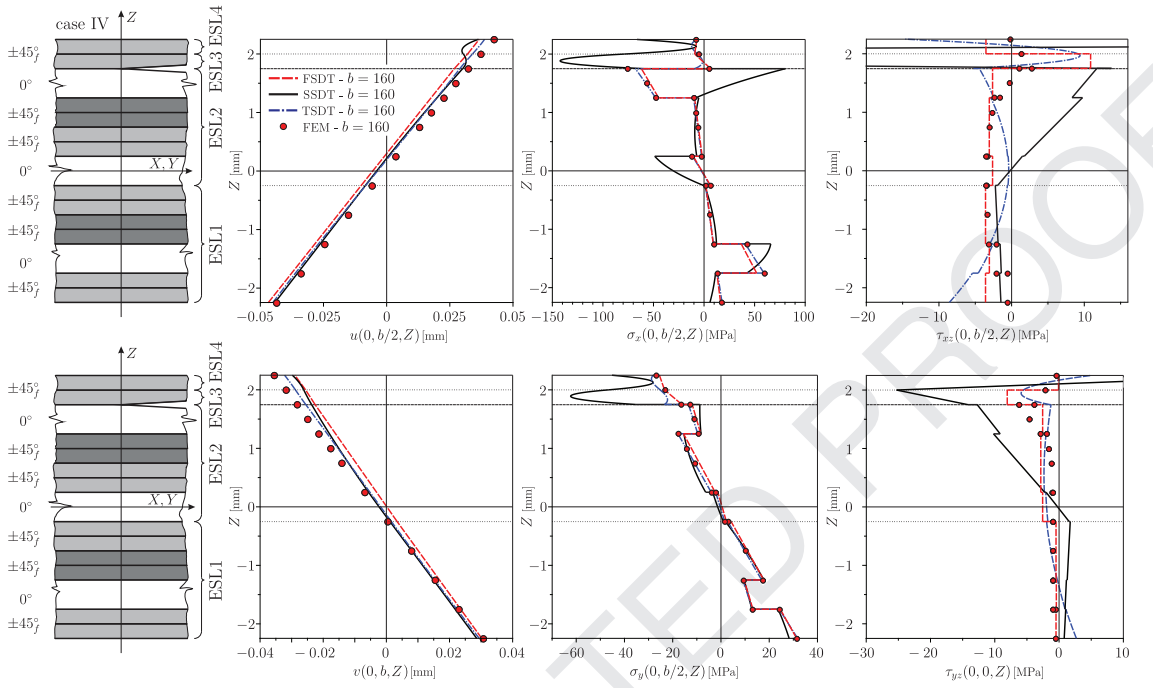

Fig. 9. Distribution of the in-plane displacements (u and v), normal stresses (σ_x and σ_y) and shear stresses (τ_{xz} and τ_{yz}) over the plate thickness for example in Fig. 4a, case IV, $b = 160$ mm.

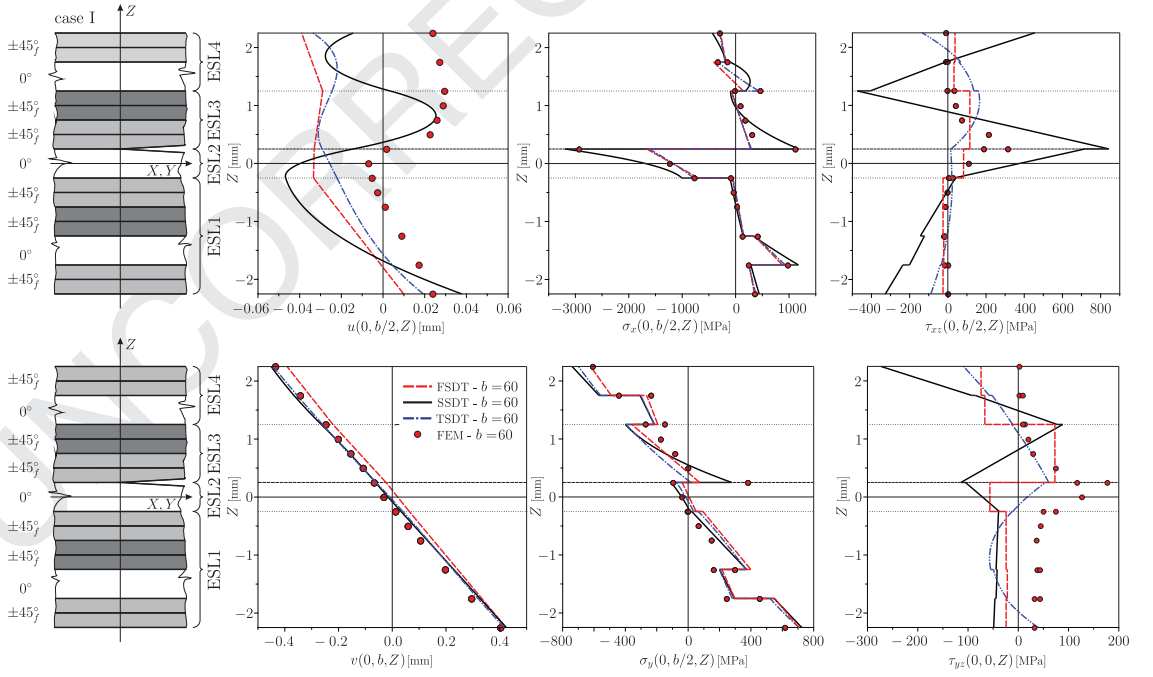

Fig. 10. Distribution of the in-plane displacements (u and v), normal stresses (σ_x and σ_y) and shear stresses (τ_{xz} and τ_{yz}) over the plate thickness for example in Fig. 4b, case I, $b = 60$ mm.

stresses are again better predicted by the SSDT than FSDT and TSDT, however with respect to the shear stresses SSDT gives unrealistic results. The FSDT or TSDT follows reasonably τ_{xz} but τ_{yz} is badly estimated by both theory. The higher perturbation of the system is the reason for the latter discrepancy compared to the FE results. The subsequent cases II, III and IV are presented in Figs. 11–13. The conclusions are in fact the same as those for problem a. It can be stated that considering both problems and all the four cases TSDT provides the best results.

Please cite this article as: A. Szekrényes, Semi-layerwise analysis of laminated plates with nonsingular delamination—The theorem of autocontinuity, Applied Mathematical Modelling (2015), http://dx.doi.org/10.1016/j.apm.2015.06.037

UNCORRECTED PROOF

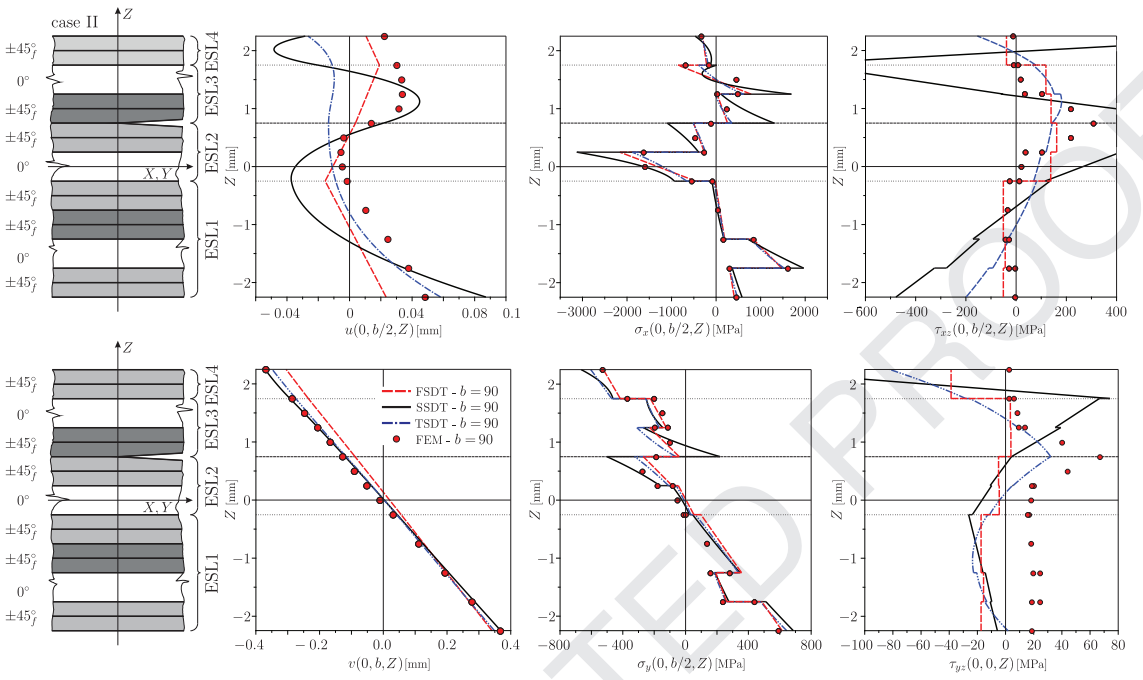

Fig. 11. Distribution of the in-plane displacements (u and v), normal stresses (σ_x and σ_y) and shear stresses (τ_{xz} and τ_{yz}) over the plate thickness for example in Fig. 4b, case II, $b = 90$ mm.

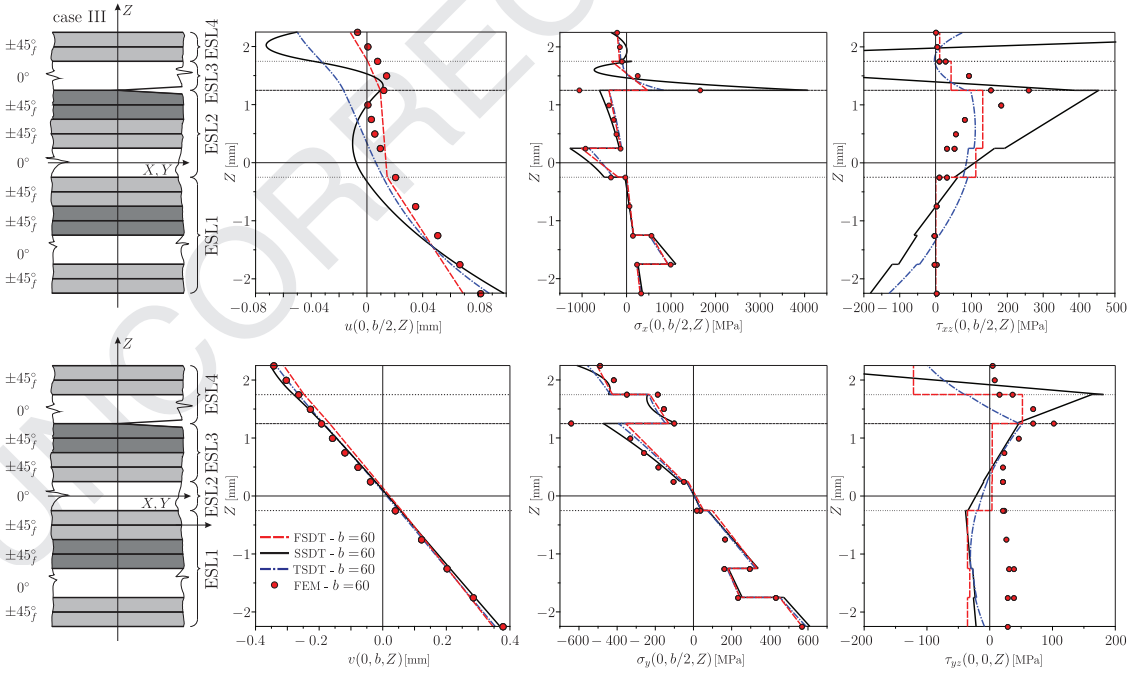

Fig. 12. Distribution of the in-plane displacements (u and v), normal stresses (σ_x and σ_y) and shear stresses (τ_{xz} and τ_{yz}) over the plate thickness for example in Fig. 4b, case III, $b = 60$ mm.

12. J-integral and mode mixity distributions

The ERR ($G_{II} = J_{II}$, $G_{III} = J_{III}$) and mode mixity distributions are plotted in Figs. 14–17 for problem a in Fig. 4. In Fig. 14 cases I and II are presented for both plate widths ($b = 100$ and $b = 160$ mm). The symbols show the results of the FE calculations by the virtual crack closure technique (VCCT) [122,139], the curves represent the analytical solutions. The results of case I shows

Please cite this article as: A. Szekrényes, Semi-layerwise analysis of laminated plates with nonsingular delamination—The theorem of autocontinuity, Applied Mathematical Modelling (2015), http://dx.doi.org/10.1016/j.apm.2015.06.037

UNCORRECTED PROOF

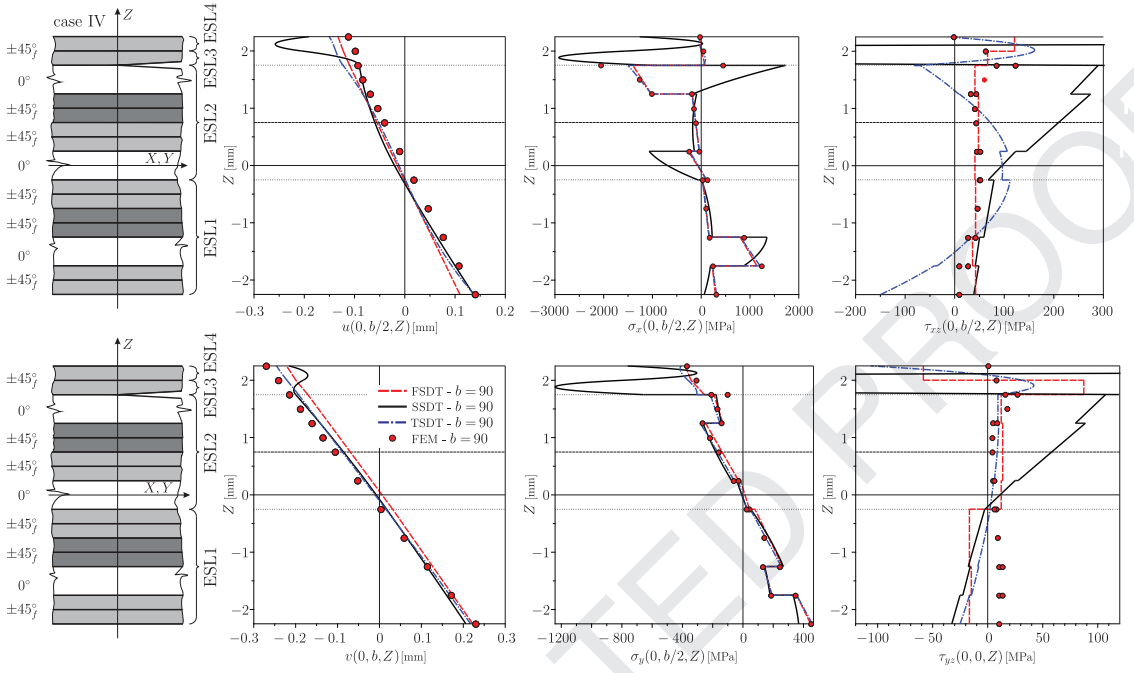

Fig. 13. Distribution of the in-plane displacements (u and v), normal stresses (σ_x and σ_y) and shear stresses (τ_{xz} and τ_{yz}) over the plate thickness for example in Fig. 4b, case IV, $b = 90$ mm.

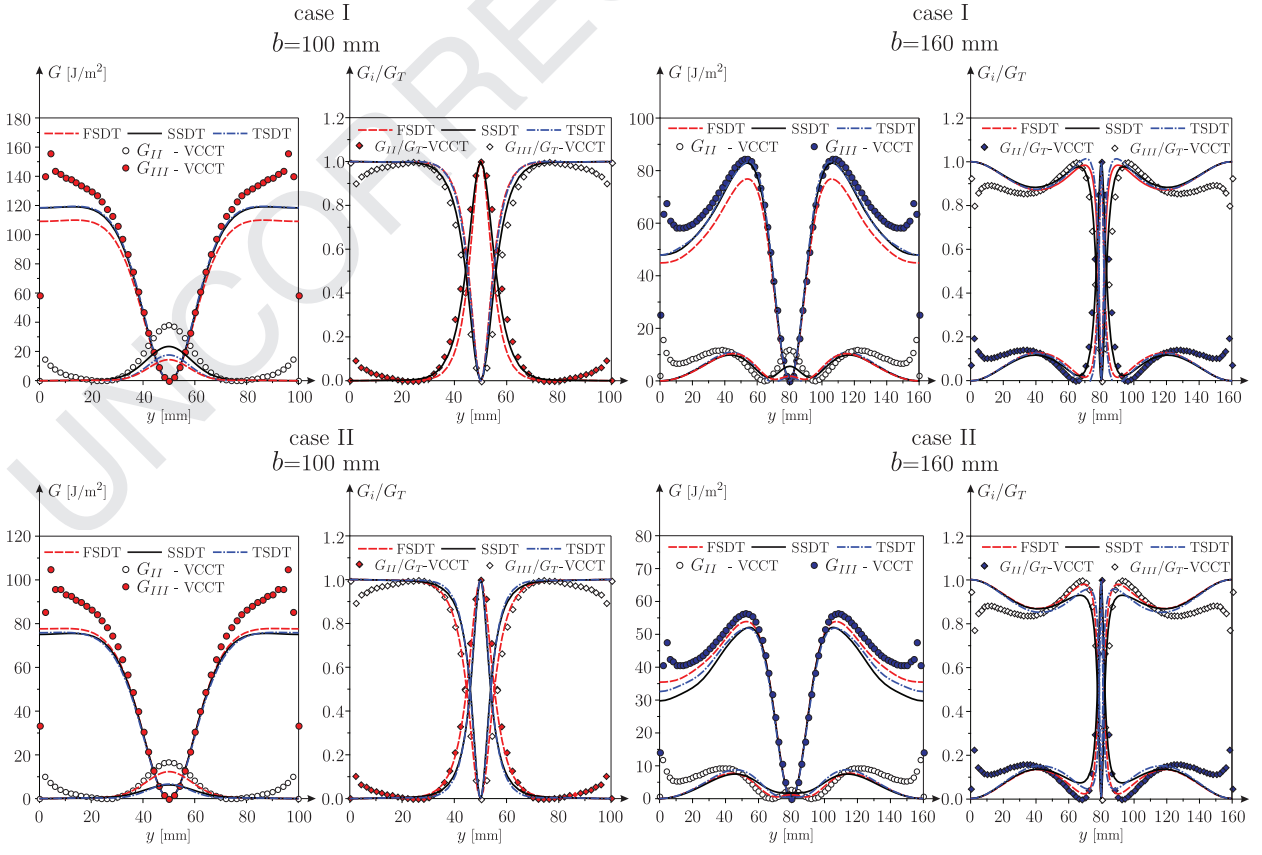

Fig. 14. Distribution of the energy release rates and mode mixity along the delamination front for example a in Fig. 4, cases I and II.

UNCORRECTED PROOF

Please cite this article as: A. Szekrényes, Semi-layerwise analysis of laminated plates with nonsingular delamination—The theorem of autocontinuity, Applied Mathematical Modelling (2015), http://dx.doi.org/10.1016/j.apm.2015.06.037

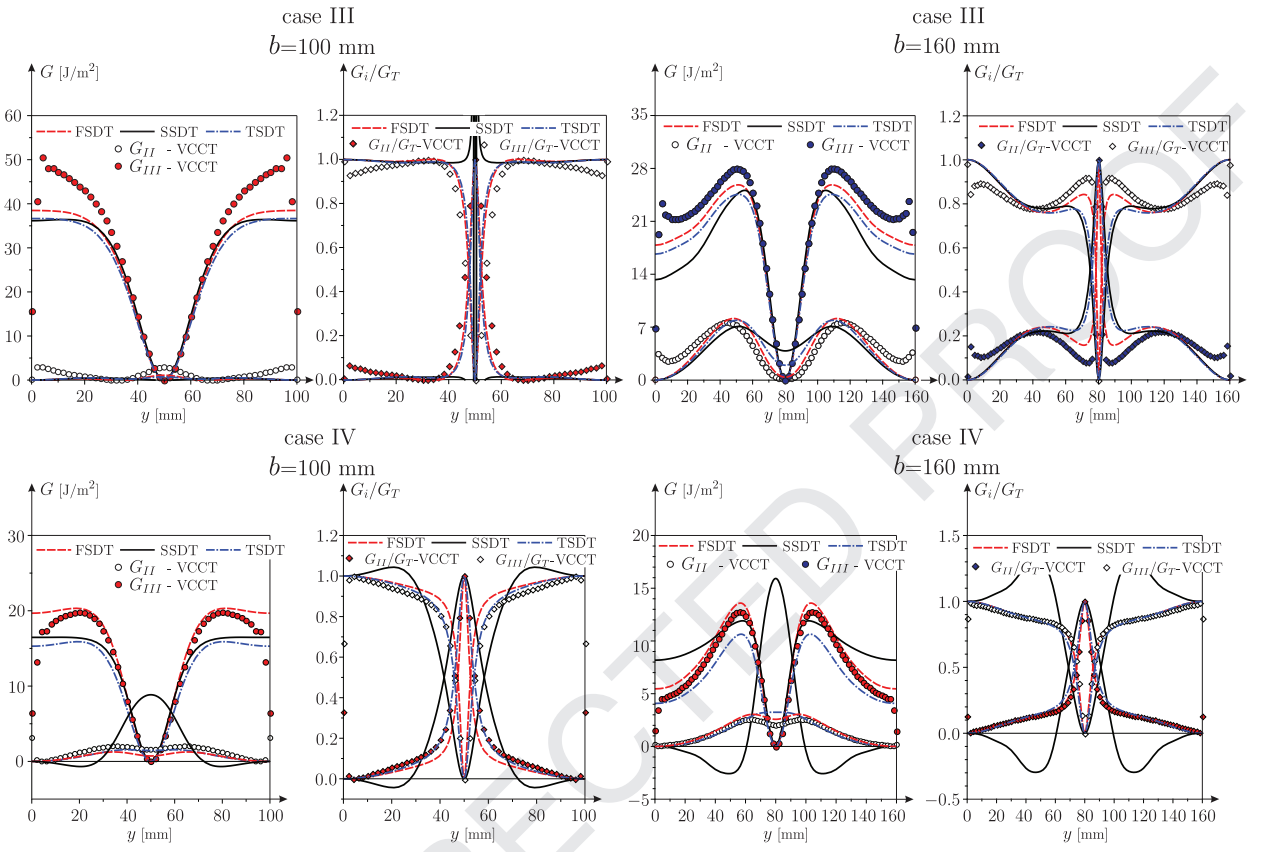

Fig. 15. Distribution of the energy release rates and mode mixity along the delamination front for example a in Fig. 4, cases III and IV.

that compared to the FE model the mode-II ERR is underpredicted by the FSDT and TSDT models if $b = 100$ mm. Although the SSDT still shows underprediction, it is obvious that it provides the best agreement with the numerical model. The mode-III ERR is captured better by the TSDT and SSDT than by FSDT. The mode mixities ($G_T = G_{II} + G_{III}$) are well predicted by each theory ($b = 100$ mm). If the plate width is $b = 160$ mm then again the SSDT is definitely the best choice, although the FSDT and TSDT theories also perform well. In case II (bottom part of Fig. 14) it is shown that the FSDT performs better than the other two theories for both plate widths.

Fig. 15 shows the results in cases III and IV for both plate widths. In case III (top half of Fig. 15) if $b = 100$ mm the three theories provide similar distributions compared to the FE results. For $b = 160$ mm the FSDT follows better the ERRs and the mode mixity than the SSDT and TSDT. It has to be mentioned that in Fig. 8 the shear stresses are erroneously captured by the SSDT. In spite of that the ERRs and mode mixities are predicted in the acceptable way by the second-order theory. In case IV (bottom half of Fig. 15) it is conspicuous that close to the edges the SSDT gives negative distribution of the mode-II ERR both plate widths. For this reason the mode mixities by SSDT are not correct. It is again surprising that in case IV the FSDT is slightly better than the TSDT in the estimation of the ERRs, even the mode ratios are better predicted by FSDT. Considering all of the cases (I–IV) in Figs. 14 and 15 (problem a) it is concluded that the FSDT approximates the numerical results with the highest accuracy among the three theories considered.

The results for problem b in Fig. 4 are displayed in Figs. 16 and 17. It has to be mentioned that the perturbation of the displacement and stress fields is significantly more intense than in the case of problem a. Therefore the agreement with the FE results is expected to be worse than in problem a. The layout of these figures is the same as that for Figs. 14 and 15. Briefly speaking, in case I the SSDT overestimates significantly the mode-III ERR for both plate widths ($b = 60$ mm and $b = 90$ mm), while the FSDT and TSDT perform with similar accuracy. Nevertheless each theory overpredicts the mode-III ERR. In case II (Fig. 16, bottom half) the performance of all three theories is similar, but SSDT seems to the best. Fig. 17 shows the results for cases III and IV. In case III (top half of Fig. 17) the **SSDT** theory seems to be the best choice, while in case IV TSDT is definitely better than the other two theories. Obviously the SSDT model is not suitable to capture the mechanical fields in case IV because the mode-II ERR distribution is negative again.

Based on the results obtained it can be concluded that the accurate description of the displacement and stress fields is very important to obtain ERR and mode mixity distributions with high accuracy. Moreover each theory gives finite stresses that is why the delamination is nonsingular in each cases. The comparison of the shear stress distributions in Figs. 6–9 to the ERR and mode mixity distributions in Figs. 14 and 15 indicates that the better the approximation of shear stresses is, the

UNCORRECTED PROOF

Please cite this article as: A. Szekrényes, Semi-layerwise analysis of laminated plates with nonsingular delamination—The theorem of autocontinuity, Applied Mathematical Modelling (2015), http://dx.doi.org/10.1016/j.apm.2015.06.037

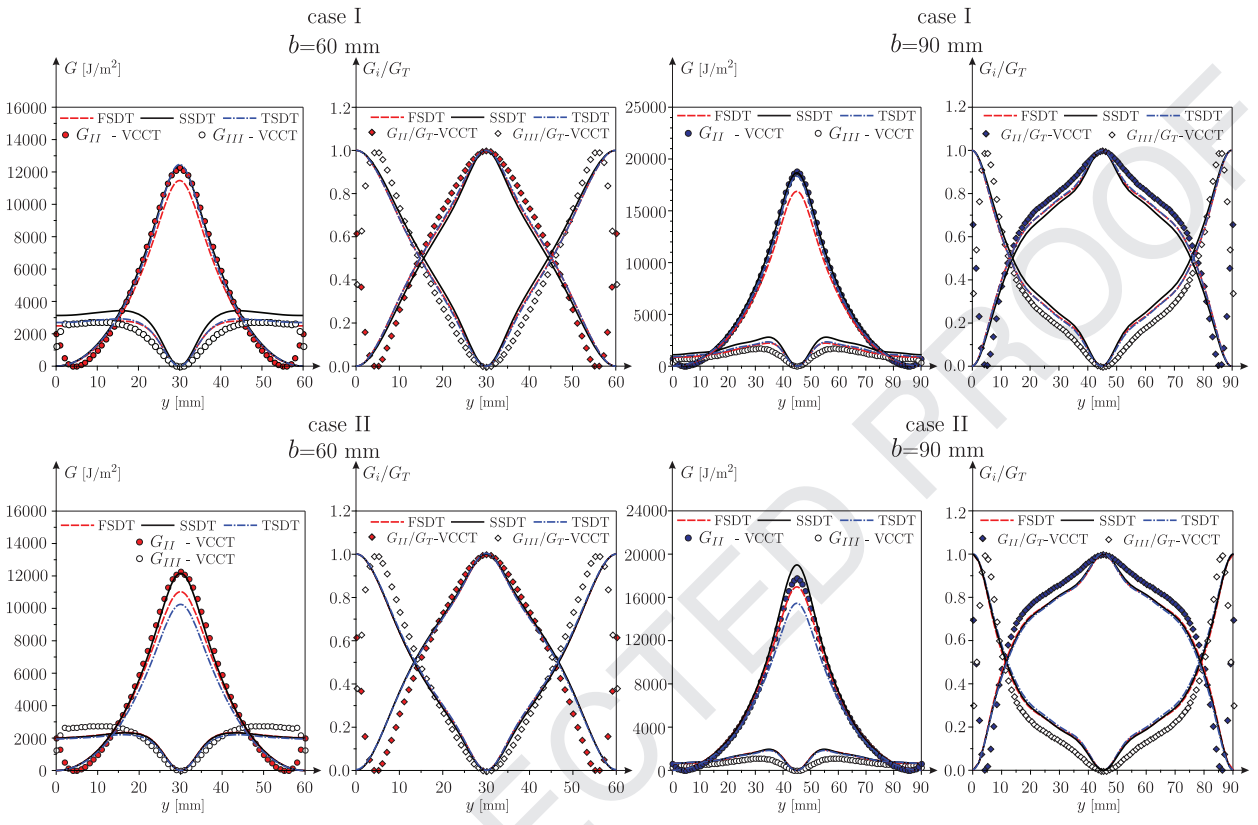

Fig. 16. Distribution of the energy release rates and mode mixity along the delamination front for example b in Fig. 4, cases I and II.

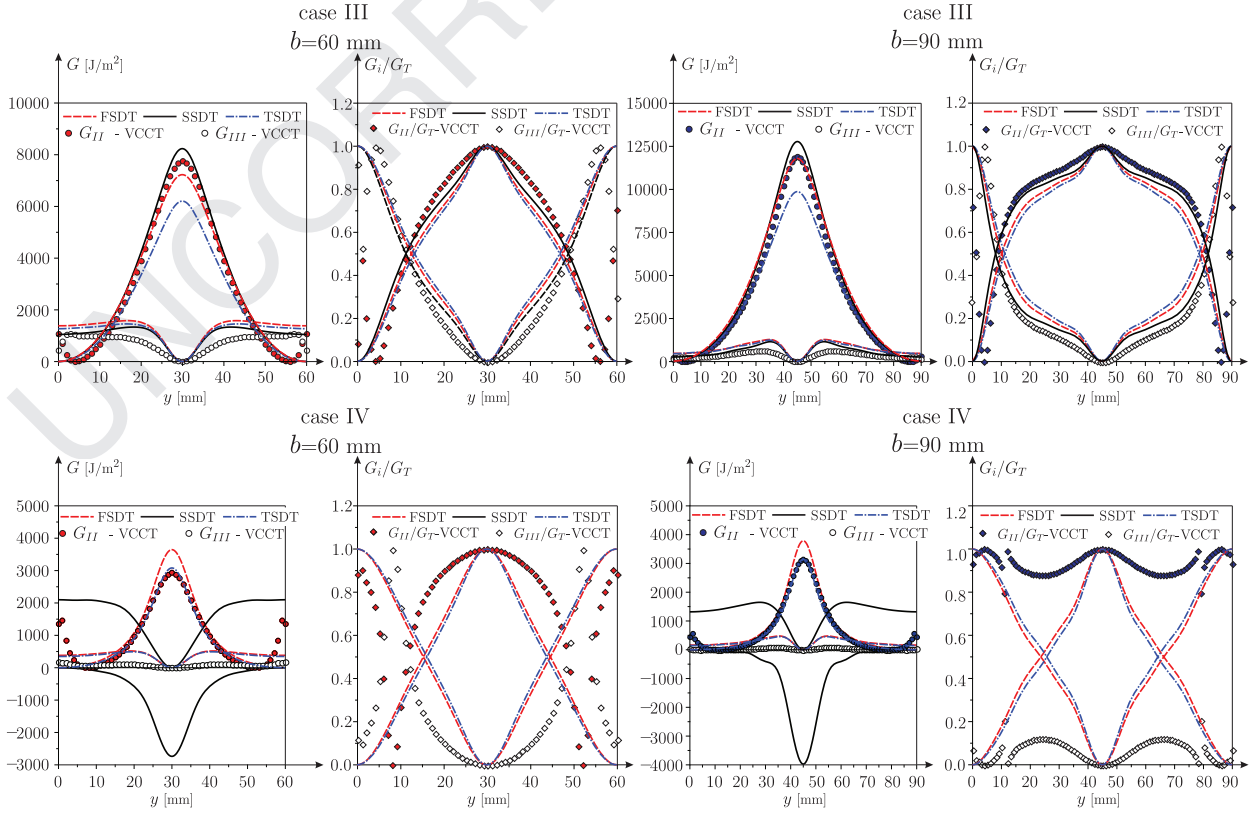

Fig. 17. Distribution of the energy release rates and mode mixity along the delamination front for example b in Fig. 4, cases III and IV.

UNCORRECTED PROOF

Please cite this article as: A. Szekrényes, Semi-layerwise analysis of laminated plates with nonsingular delamination—The theorem of autocontinuity, Applied Mathematical Modelling (2015), http://dx.doi.org/10.1016/j.apm.2015.06.037

higher the accuracy of the approximation of the ERRs is. The final conclusion is that for problem a the FSDT theory gives the best approximation of the numerical results. In contrast, for problem b the TSDT theory should be highlighted, especially in case IV.

13. Conclusions

The method of four equivalent single layers is presented in this paper for the modeling of delaminated orthotropic composite plates. The in-plane displacement functions were captured by the first-, second- and third-order plate theories. The problem of a plate with straight delamination front was considered, each region was captured by four equivalent single layers. The kinematic continuity between the equivalent single layers was established by the system of exact kinematic conditions. It is important to note that the set of conditions was complemented with the continuity of the derivative and the curvature of the shear strains between the adjacent layers of third-order plates. With the aid of the kinematic conditions the number of parameters in the displacement functions was reduced significantly. The strain and stress fields were derived using the basic equations of elasticity. The equilibrium equations of the delaminated and undelaminated parts were derived based on variational calculus. To exemplify the developed models simply supported layered plates were considered with concentrated load. The problems were solved by the state-space approach.

An important contribution of this paper compared to similar previous developments is the introduction of the theorem of autocontinuity (AC theorem) for second- and third-order plates. Because of the parameter elimination the number of parameters in the displacement field that continuity is required against is higher than the available constants in the state-space model. Thus, there are no free constants for the matching of certain second- and third-order displacement parameters. However, in accordance with the AC theorem the continuity of these parameters can be achieved by imposing the continuity of certain autocontinuity (AC) parameters. An important requirement is that the autocontinuity is satisfied only if in each interface plane between the adjacent equivalent single layers the same conditions are imposed in the delaminated and undelaminated plate regions, except for the plane of delamination, where different conditions are necessary to be specified because of the presence of the delamination front. Using the proposed conditions and the AC theorem the examples were solved and the mechanical fields were compared to the results of 3D finite element calculations. It was shown that in problem a, very good agreement was achieved with the numerical results. The energy release rate and the mode mixity were predicted by the FSDT in the best way. Apparently the disadvantage of the theories were discovered through problem b, for which the TSDT theory was the best choice. In this example the more intense perturbation led to the fact that the analytical models gave inaccurate results.In spite of that, the updated system of exact kinematic conditions and the theorem of autocontinuity work well and can be implemented into more accurate plate (and even beam and shell) theories. Also, it was discussed that the dynamic boundary condition is important to be satisfied by an accurate plate model. However, in the method of four equivalent single layers these conditions make the model over-constrained leading to continuity problems between the delaminated and undelaminated portions, and thus these were not considered in this work.

More work is required to solve the benchmark problems discussed with higher accuracy and to find a model to be the candidate for the development of a plate/shell finite element in the delamination modeling of composite plates, which can replace the computationally expensive 3D model and the VCCT. As a matter of fact there are numerous refined models [118–120,140–145] that can be tried out before the final decision.

Acknowledgments

This work was supported by the János Bolyai Research Scholarship of the Hungarian Academy of Sciences and the Hungarian National Scientific Research Fund (OTKA) under grant no. 44615-066-15 (108414).

Appendix A. TSDT constants

In this Appendix the nonzero constants in Eq. (13) denoted by $K_{ij}^{(0)}$, $K_{ij}^{(2)}$ and $K_{ij}^{(3)}$ are collected.

A1. Undelaminated region

In accordance with Section 4.1.1 the following constants can be obtained:

$$K_{11}^{(0)} = -\frac{1}{12}\frac{(t_1+t_2+2z_R^{(2)})(5t_2^2+7t_1t_2-10z_R^{(2)}t_2+8(z_R^{(2)})^2+2t_1^2-4z_R^{(2)}t_1)}{(t_1+2t_2)(t_1+t_2)}$$

$$K_{12}^{(0)} = -\frac{1}{12}\frac{(t_1+t_2+2z_R^{(2)})^2(t_1+4t_2-4z_R^{(2)})^2}{t_2(t_1+t_2)}$$

$$K_{13}^{(0)} = \frac{1}{12}\frac{(t_1+t_2+2z_R^{(2)})^2(t_1+t_2-4z_R^{(2)})(2t_3+t_4)}{t_2(t_1+2t_2)(t_3+t_4)}$$

Please cite this article as: A. Szekrényes, Semi-layerwise analysis of laminated plates with nonsingular delamination—The theorem of autocontinuity, Applied Mathematical Modelling (2015), http://dx.doi.org/10.1016/j.apm.2015.06.037

UNCORRECTED PROOF

$$K_{14}^{(0)} = -\frac{1}{12}\frac{(t_1+t_2+2z_R^{(2)})^2(t_1+t_2-4z_R^{(2)})t_3}{t_2(t_1+2t_2)(t_3+t_4)}$$
$$K_{15}^{(0)} = \frac{1}{16}\frac{(t_1+t_2+2z_R^{(2)})^2(t_1+t_2-4z_R^{(2)})t_3(2t_3+t_4)}{t_2(t_1+2t_2)} \tag{A.1}$$

$$K_{21}^{(0)} = \frac{1}{3}\frac{(3t_2-4z_R^{(2)})(z_R^{(2)})^2}{(t_1+2t_2)(t_1+t_2)}, \quad K_{22}^{(0)} = -\frac{1}{3}\frac{(3t_1t_2-3t_1z_R^{(2)}-4(z_R^{(2)})^2+3t_2^2)z_R^{(2)}}{t_2(t_1+t_2)}$$
$$K_{23}^{(0)} = -\frac{1}{3}\frac{(2t_3+t_4)(3t_1+3t_2+4z_R^{(2)})(z_R^{(2)})^2}{t_2(t_3+t_4)(t_1+2t_2)}, \quad K_{24}^{(0)} = \frac{1}{3}\frac{(3t_1+3t_2+4z_R^{(2)})t_3(z_R^{(2)})^2}{t_2(t_3+t_4)(t_1+2t_2)}$$
$$K_{25}^{(0)} = -\frac{1}{4}\frac{t_3(2t_3+t_4)(3t_1+3t_2+4z_R^{(2)})(z_R^{(2)})^2}{t_2(t_1+2t_2)} \tag{A.2}$$

$$K_{31}^{(0)} = -\frac{1}{12}\frac{(t_2+4z_R^{(2)})(t_2-2z_R^{(2)})^2}{(t_1+2t_2)(t_1+t_2)}, \quad K_{32}^{(0)} = \frac{1}{12}\frac{(t_2-2z_R^{(2)})^2(3t_1+4t_2+4z_R^{(2)})}{t_2(t_1+2t_2)}$$
$$K_{33}^{(0)} = \frac{1}{12}\left(\frac{(10t_3+5t_4)t_2^3+(3t_1t_4+6t_1t_3+12t_4t_3+18t_3^2)t_2^2+(-(12t_4+24t_3)(z_R^{(2)})^2}{t_2(t_3+t_4)(t_1+2t_2)}\right.$$
$$\left.+\frac{6t_1t_4t_3+9t_1t_3^2)t_2-4(z_R^{(2)})^2(2t_1+t_2)(3t_1+z_R^{(2)})}{t_2(t_3+t_4)(t_1+2t_2)}\right)$$
$$K_{34}^{(0)} = -\frac{t_3}{12}\frac{(5t_2^3+(3t_1+6t_3)t_2^2+(3t_1t_3-12(z_R^{(2)})^2)t_2-4(z_R^{(2)})^2(4z_R^{(2)}+3t_1)}{t_2(t_1+2t_2)(t_3+t_4)}$$
$$K_{35}^{(0)} = \frac{t_3}{16}\left(\frac{(10t_3+5t_4)t_2^3+(6t_1t_3+10t_3^2+3t_1t_4+6t_4t_3)t_2^2+(-(12t_4+24t_3)(z_R^{(2)})^2}{t_2(t_3+t_4)(t_1+2t_2)}\right.$$
$$\left.+\frac{3t_1t_4t_3+5t_1t_3^2)t_2-4(z_R^{(2)})^2(2t_3+t_4)(3t_1+4z_R^{(2)})}{t_2(t_3+t_4)(t_1+2t_2)}\right) \tag{A.3}$$

$$K_{41}^{(0)} = -\frac{1}{12}\frac{(t_2+4z_R^{(2)})(t_2-2z_R^{(2)})^2}{(t_1+2t_2)(t_1+t_2)}, \quad K_{42}^{(0)} = \frac{1}{12}\frac{(4t_2+3t_1+4z_R^{(2)})(t_2-4z_R^{(2)})^2}{t_2(t_1+t_2)}$$
$$K_{43}^{(0)} = \frac{1}{12}\left(\frac{(2t_3+t_4)(5t_2^3+3(4t_3+t_1+2t_4)t_2^2+3(t_1t_4+t_1t_3-4(z_R^{(2)})^2)t_2}{t_2(t_1+2t_2)(t_3+t_4)}+\frac{-4(z_R^{(2)})^2(4z_R^{(2)}+3t_1)}{t_2(t_1+2t_2)(t_3+t_4)}\right) \tag{A.4}$$

$$K_{44}^{(0)} = -\frac{1}{12}\left(\frac{5t_2^3t_3+3(t_1t_3-4t_4t_3-2t_4^2)t_2^2+3(-t_1t_4^2-2t_1t_3t_4-4t_3(z_R^{(2)})^2)t_2}{t_2(t_1+2t_2)(t_3+t_4)}-\frac{4t_3(z_R^{(2)})^2(4z_R^{(2)}+3t_1)}{t_2(t_1+2t_2)(t_3+t_4)}\right)$$
$$K_{45}^{(0)} = \frac{1}{16}\frac{(2t_3+t_4)(5t_2^3t_3+(3t_1t_3-2t_3t_4+4t_3^2-2t_4^2)t_2^2}{t_2(t_1+2t_2)}$$
$$+\frac{(2t_1t_3^2-t_1t_3t_4-12t_3(z_R^{(2)})^2-t_1t_4^2)t_2-4t_3(z_R^{(2)})^2(4z_R^{(2)}+3t_1)}{t_2(t_1+2t_2)} \tag{A.5}$$

$$K_{11}^{(2)} = -\frac{(3t_2+2t_1)}{(t_1+2t_2)(t_1+t_2)}, \quad K_{12}^{(2)} = -\frac{(t_1+2t_2)}{t_2(t_1+t_2)}, \quad K_{13}^{(2)} = -\frac{(2t_3+t_4)(t_1+t_2)}{t_2(t_3+t_4)(t_1+2t_2)},$$
$$K_{14}^{(2)} = -\frac{(t_1+t_2)t_3}{t_2(t_1+2t_2)(t_3+t_4)}, \quad K_{15}^{(2)} = -\frac{3}{4}\frac{t_3(2t_3+t_4)(t_1+t_2)}{t_2(t_1+2t_2)} \tag{A.6}$$

$$K_{21}^{(2)} = -\frac{t_2}{(t_1+2t_2)(t_1+t_2)}, \quad K_{22}^{(2)} = -\frac{t_1}{t_2(t_1+t_2)}, \quad K_{23}^{(2)} = -K_{13}^{(2)},$$
$$K_{24}^{(2)} = -K_{14}^{(2)}, \quad K_{25}^{(2)} = -K_{15}^{(2)} \tag{A.7}$$

$$K_{33}^{(2)} = -\frac{1}{(t_3+t_4)}, \quad K_{34}^{(2)} = \frac{1}{(t_3+t_4)}, \quad K_{35}^{(2)} = -\frac{3}{4}(t_3+t_4)$$
$$K_{43}^{(2)} = K_{33}^{(2)}, \quad K_{44}^{(2)} = K_{34}^{(2)}, \quad K_{45}^{(2)} = -K_{35}^{(2)} \tag{A.8}$$

Please cite this article as: A. Szekrényes, Semi-layerwise analysis of laminated plates with nonsingular delamination—The theorem of autocontinuity, Applied Mathematical Modelling (2015), http://dx.doi.org/10.1016/j.apm.2015.06.037

UNCORRECTED PROOF

$$K_{11}^{(3)} = K_{21}^{(3)} = \frac{4}{3(t_1+2t_2)(t_1+t_2)}, \quad K_{12}^{(3)} = K_{22}^{(3)} = -\frac{4}{3t_2(t_1+t_2)},$$
$$K_{13}^{(3)} = K_{23}^{(3)} = \frac{4}{3}\frac{2t_3+t_4}{t_2(t_1+2t_2)(t_3+t_4)}, \quad K_{14}^{(3)} = K_{24}^{(3)} = -\frac{4}{3}\frac{t_3}{t_2(t_1+2t_2)(t_3+t_4)},$$
$$K_{15}^{(3)} = K_{25}^{(3)} = \frac{(2t_3+t_4)t_3}{t_2(t_1+2t_2)}, \quad K_{35}^{(3)} = K_{45}^{(3)} = 1 \tag{A.9}$$

A2. Delaminated region

Based on Section 4.2.1 the following constants can be derived:

$$K_{11}^{(0)} = -\frac{1}{4}\frac{t_2(2t_1+t_2)}{(t_1+t_2)}, \quad K_{12}^{(0)} = -\frac{1}{4}\frac{t_2^2}{(t_1+t_2)}, \quad K_{15}^{(0)} = \frac{1}{16}(3t_1+t_2)t_2^2 \tag{A.10}$$

$$K_{21}^{(0)} = \frac{1}{4}\frac{t_1^2}{(t_1+t_2)}, \quad K_{22}^{(0)} = \frac{1}{4}\frac{t_1(t_1+2t_2)}{(t_1+t_2)}, \quad K_{25}^{(0)} = -\frac{1}{16}(t_1+3t_2)t_1^2 \tag{A.11}$$

$$K_{33}^{(0)} = -\frac{1}{4}\frac{t_4(2t_3+t_4)}{(t_3+t_4)}, \quad K_{34}^{(0)} = -\frac{1}{4}\frac{t_4^2}{(t_3+t_4)}, \quad K_{36}^{(0)} = \frac{1}{16}(3t_3+t_4)t_4^2 \tag{A.12}$$

$$K_{43}^{(0)} = \frac{1}{4}\frac{t_3^2}{(t_3+t_4)}, \quad K_{44}^{(0)} = \frac{1}{4}\frac{t_3(t_3+2t_4)}{(t_3+t_4)}, \quad K_{46}^{(0)} = -\frac{1}{16}(t_3+3t_4)t_2^2 \tag{A.13}$$

$$K_{11}^{(2)} = K_{21}^{(2)} = -\frac{1}{(t_1+t_2)}, \quad K_{12}^{(2)} = K_{22}^{(2)} = \frac{1}{(t_1+t_2)}, \quad K_{15}^{(2)} = -K_{25}^{(2)} = -\frac{3}{4}(t_1+t_2),$$
$$K_{33}^{(2)} = K_{43}^{(2)} = -\frac{1}{(t_3+t_4)}, \quad K_{34}^{(2)} = K_{44}^{(2)} = \frac{1}{(t_3+t_4)}, \quad K_{36}^{(2)} = -K_{46}^{(2)} = -\frac{3}{4}(t_3+t_4) \tag{A.14}$$

$$K_{15}^{(3)} = K_{25}^{(3)} = 1, \quad K_{36}^{(3)} = K_{46}^{(3)} = 1 \tag{A.15}$$

Appendix B. SSDT constants

B1. Undelaminated region

On the base of the explanation in Section 4.1.2 the SSDT constants become:

$$K_{11}^{(0)} = -\frac{1}{4}t_1, \quad K_{12}^{(0)} = -\frac{1}{4}\frac{t_2(2t_1+3t_2)+4z_R^{(2)}(t_2-z_R^{(2)})}{t_2}$$
$$K_{13}^{(0)} = \frac{1}{4}\frac{(t_1t_2-4(z_R^{(2)})^2+t_2^2)}{t_2}, \quad K_{15}^{(0)} = -\frac{t_3}{4}\frac{(t_1t_2-4(z_R^{(2)})^2+t_2^2)}{t_2} \tag{B.1}$$

$$K_{22}^{(0)} = -\frac{z_R^{(2)}(t_2-4z_R^{(2)})}{t_2}, \quad K_{23}^{(0)} = -\frac{(z_R^{(2)})^2}{t_2}, \quad K_{25}^{(0)} = t_3\frac{(z_R^{(2)})^2}{t_2}$$
$$K_{32}^{(0)} = \frac{1}{4}\frac{(t_2-2z_R^{(2)})^2}{t_2}, \quad K_{33}^{(0)} = \frac{1}{4}\frac{-4(z_R^{(2)})^2+t_2^2+2t_3t_2}{t_2}, \quad K_{35}^{(0)} = -\frac{t_3}{4}\frac{(t_3t_2+t_2^2-4(z_R^{(2)})^2)}{t_2}$$
$$K_{42}^{(0)} = K_{32}^{(0)}, \quad K_{43}^{(0)} = \frac{1}{4}\frac{(t_2^2+t_2t_4+4t_3t_2-4(z_R^{(2)})^2)}{t_2}, \quad K_{44}^{(0)} = \frac{1}{4}t_4, \quad K_{45}^{(0)} = -\frac{t_3}{4}\frac{(t_4t_2+t_2^2-4(z_R^{(2)})^2)}{t_2} \tag{B.2}$$

$$K_{11}^{(2)} = K_{13}^{(2)} = -\frac{1}{t_1}, \quad K_{12}^{(2)} = \frac{2}{t_1}, \quad K_{15}^{(2)} = \frac{t_3}{t_1}, \quad K_{22}^{(2)} = -\frac{1}{t_2}, \quad K_{23}^{(2)} = \frac{1}{t_2}$$
$$K_{25}^{(2)} = -\frac{t_3}{t_2}K_{35}^{(2)} = 1, \quad K_{43}^{(2)} = -K_{44}^{(2)} = -\frac{1}{t_4}, \quad K_{45}^{(2)} = -\frac{t_3}{t_4} \tag{B.3}$$

B2. Delaminated region

In accordance with Section 4.2.2 we have:

$$K_{11}^{(0)} = -\frac{1}{2}t_2, \quad K_{15}^{(0)} = -\frac{1}{4}t_2^2, \quad K_{21}^{(0)} = \frac{1}{4}(2t_1+t_2), \quad K_{22}^{(0)} = \frac{1}{4}t_2, \quad K_{25}^{(0)} = \frac{1}{4}(t_1^2-t_2^2+t_1t_2)$$
$$K_{33}^{(0)} = -\frac{1}{2}t_4, \quad K_{36}^{(0)} = -\frac{1}{4}t_4^2, \quad K_{43}^{(0)} = \frac{1}{4}(2t_3-t_4), \quad K_{44}^{(0)} = \frac{1}{4}t_4, \quad K_{46}^{(0)} = \frac{1}{4}(t_3t_4+t_3^2-t_4^2) \tag{B.4}$$

Please cite this article as: A. Szekrényes, Semi-layerwise analysis of laminated plates with nonsingular delamination—The theorem of autocontinuity, Applied Mathematical Modelling (2015), http://dx.doi.org/10.1016/j.apm.2015.06.037

UNCORRECTED PROOF

$$K_{15}^{(2)}=1,\quad K_{21}^{(2)}=-K_{22}^{(2)}=-\frac{1}{t_2},\quad K_{25}^{(2)}=-\frac{t_1}{t_2}$$
$$K_{36}^{(2)}=1,\quad K_{43}^{(2)}=-K_{44}^{(2)}=\frac{1}{t_4},\quad K_{46}^{(2)}=-\frac{t_3}{t_4} \tag{B.5}$$

Appendix C. FSDT constants

C1. Undelaminated part

The explanation in Section 4.1.3 provides the following:

$$K_{11}^{(0)}=-\frac{1}{2}t_1,\quad K_{12}^{(0)}=-z_R^{(2)}-\frac{1}{2}t_2,\quad K_{22}^{(0)}=-z_R^{(2)},\quad K_{32}^{(0)}=-z_R^{(2)}-\frac{1}{2}t_2$$
$$K_{33}^{(0)}=\frac{1}{2}t_3,\quad K_{42}^{(0)}=-z_R^{(2)}+\frac{1}{2}t_2,\quad K_{43}^{(0)}=t_3,\quad K_{44}^{(0)}=\frac{1}{2}t_3 \tag{C.1}$$

C2. Delaminated region

According to Section 4.2.3 the following constants can be obtained:

$$K_{11}^{(0)}=-\frac{1}{2}t_2,\quad K_{21}^{(0)}=\frac{1}{2}(t_1-t_2),\quad K_{22}^{(0)}=\frac{1}{2}t_2$$
$$K_{33}^{(0)}=-\frac{1}{2}t_4,\quad K_{43}^{(0)}=\frac{1}{2}(t_3-t_4),\quad K_{44}^{(0)}=\frac{1}{2}t_4 \tag{C.2}$$

Appendix D. B.C.s and C.C.s for SSDT and FSDT

The B.C.s of SSDT can be defined by replacing λ with ϕ and P with L in Eqs. (36)–(39). The equivalent bending moments are given by Eqs. (40) and (42) with $K_{ij}^{(3)}=0$, moreover the equivalent higher-order stress resultants become:

$$\hat{\mathbf{L}}_1^{(x,y)(1)}=\sum_{j=1,2}\left(K_{j5}^{(0)}\mathbf{N}_j^{(x,xy)}+K_{j5}^{(2)}\mathbf{L}_j^{(x,xy)}\right)^{(1)},\quad \hat{\mathbf{L}}_3^{(x,y)(1)}=\sum_{j=3,4}\left(K_{j6}^{(0)}\mathbf{N}_j^{(x,xy)}+K_{j6}^{(2)}\mathbf{L}_j^{(x,xy)}\right)^{(1)} \tag{D.1}$$

$$\hat{\mathbf{L}}_3^{(x,y)(2)}=\sum_{j=1..4}\left(K_{j5}^{(0)}\mathbf{N}_j^{(x,xy)}+K_{j5}^{(2)}\mathbf{L}_j^{(x,xy)}\right)^{(2)} \tag{D.2}$$

The continuity of stress resultants requires:

$$\left(\hat{\mathbf{M}}_i^{(x,xy)},\frac{\hat{\mathbf{L}}_1^{(x,y)}}{t_1}+\frac{\hat{\mathbf{L}}_3^{(x,y)}}{t_3},\sum_{i=1..4}\mathbf{N}_i^{(x,xy)}\right)^{(1)}\Bigg|_{x=-0}=\left(\hat{\mathbf{M}}_i^{(x,xy)},\frac{\hat{\mathbf{L}}_3^{(x,y)}}{t_3},\sum_{i=1..4}\mathbf{N}_i^{(x,xy)(2)}\right)\Bigg|_{x=+0}, \tag{D.3}$$

where $i=1..4$. The displacement continuity can be defined by replacing λ with ϕ in Eq. (46). Moreover, the continuity of the second-order terms is imposed by:

$$\phi_{p1}\big|_{x=+0}^{(1)}=\sum_{j=1..5}K_{1j}^{(3)}\psi_{(p)j}\Big|_{x=-0}^{(2)},\quad p=x,y. \tag{D.4}$$

Between regions (1)–(1q) and (1q)–(1a) we can replace λ with ϕ and P with L in Eqs. (58) and (59) and impose the conditions by Eqs. (60) and (61). Finally, the conditions of the FSDT can be derived by ignoring ϕ, λ in the former displacement parameters; moreover L and P in the stress resultants, i.e. only membrane displacements, rotations, normal forces and bending moments should be continuous at $x=0$.

Appendix E. J-integral – mode-II and mode-III ERRs

The J-integral has already been derived in previous papers [106,114,125,126] for similar problems to those considered in this paper. The mode-II and mode-III integrals are:

$$J_{II}=\frac{1}{2}\sum_{i=1..4}\left\{\left(N_{x1(i)}\varepsilon_{x1(i)}^{(0)}\big|_{x=+0}-N_{x2(i)}\varepsilon_{x2(i)}^{(0)}\big|_{x=-0}\right)-\left(N_{y1(i)}\varepsilon_{y1(i)}^{(0)}\big|_{x=+0}-N_{y2(i)}\varepsilon_{y2(i)}^{(0)}\big|_{x=-0}\right)\right.$$
$$\left.+\left(M_{x1(i)}\varepsilon_{x1(i)}^{(1)}\big|_{x=+0}-M_{x2(i)}\varepsilon_{x2(i)}^{(1)}\big|_{x=-0}\right)-\left(M_{y1(i)}\varepsilon_{y1(i)}^{(1)}\big|_{x=+0}-M_{y2(i)}\varepsilon_{y2(i)}^{(2)}\big|_{x=-0}\right)\right.$$

Please cite this article as: A. Szekrényes, Semi-layerwise analysis of laminated plates with nonsingular delamination—The theorem of autocontinuity, Applied Mathematical Modelling (2015), http://dx.doi.org/10.1016/j.apm.2015.06.037

UNCORRECTED PROOF

$$+\left(L_{x1(i)}\varepsilon^{(2)}_{x1(i)}\big|_{x=+0}-L_{x2(i)}\varepsilon^{(2)}_{x2(i)}\big|_{x=-0}\right)-\left(L_{y1(i)}\varepsilon^{(2)}_{y1(i)}\big|_{x=+0}-L_{y2(i)}\varepsilon^{(2)}_{y2(i)}\big|_{x=-0}\right)$$
$$+\left(P_{x1(i)}\varepsilon^{(3)}_{x1(i)}\big|_{x=+0}-P_{x2(i)}\varepsilon^{(3)}_{x2(i)}\big|_{x=-0}\right)-\left(P_{y1(i)}\varepsilon^{(3)}_{y1(i)}\big|_{x=+0}-P_{y2(i)}\varepsilon^{(3)}_{y2(i)}\big|_{x=-0}\right)\Big\} \quad \text{(E.1)}$$

$$J_{III}=\frac{1}{2}\sum_{i=1..4}\Big\{\left(N_{xy1(i)}\hat{\gamma}^{(0)}_{xy1(i)}\big|_{x=+0}-N_{xy2(i)}\hat{\gamma}^{(0)}_{xy2(i)}\big|_{x=-0}\right)+\left(M_{xy1(i)}\hat{\gamma}^{(1)}_{xy1(i)}\big|_{x=+0}-M_{xy2(i)}\hat{\gamma}^{(1)}_{xy2(i)}\big|_{x=-0}\right)$$
$$+\left(L_{xy1(i)}\hat{\gamma}^{(2)}_{xy1(i)}\big|_{x=+0}-L_{xy2(i)}\hat{\gamma}^{(2)}_{xy2(i)}\big|_{x=-0}\right)+\left(P_{xy1(i)}\hat{\gamma}^{(3)}_{xy1(i)}\big|_{x=+0}-P_{xy2(i)}\hat{\gamma}^{(3)}_{xy2(i)}\big|_{x=-0}\right)\Big\}, \quad \text{(E.2)}$$

where the notations can be found in the former papers.

References

[1] D.F. Adams, L.A. Carlsson, R.B. Pipes, Experimental Characterization of Advanced Composite Materials, third ed., CRC Press, Boca Raton, London, New York, Washington, D.C., 2000.
[2] W. Zhou, X. Liang, Y. Li, S. You, R. Liu, H. Chai, Z. Lv, Acoustic emission monitoring for delaminated composites under bending damage failure condition, Appl. Mech. Mater. 310 (2013) 51–54.
[3] W. Zhou, L. Zhi-Hui, Y.-R. Wang, R. Liu, W.-Y. Chen, X.-T. Li, Acoustic response and micro-damage mechanism of fiber composite materials under mode-II delamination, Chinese Phys. Lett. 32 (2015) 046201.
[4] R.A. Chaudhuri, K. Balaraman, A novel method for fabrication of fiber reinforced plastic laminated plates, Compos. Structures 77 (2007) 160–170.
[5] I.D. Baere, W.V. Paepegem, J. Degrieck, Feasibility study of fusion bonding for carbon fabric reinforced polyphenylene sulphide by hot-tool welding, J. Thermoplastic Compos. Mater. 25 (2012) 135–151.
[6] K. Allaer, I.D. Baere, W.V. Paepegem, J. Degrieck, Infrared welding of carbon fabric reinforced thermoplastics, JEC Compos. Mag. 77 (2012) 44–47.
[7] T. Czigány, T. Deák, Preparation and manufacturing techniques for macro- and microcomposites, Polymer Compos. 1 (2012) 111–134.
[8] L. Mészáros, T. Deák, G. Balogh, T. Czvikovszky, T. Czigány, Preparation and mechanical properties of injection moulded polyamide 6 matrix hybrid nanocomposite, Compos. Sci. Technol. 75 (2013) 22–27.
[9] V. Rizov, A. Shipsha, D. Zenkert, Indentation study of foam core sandwich composite panels, Compos. Struct. 69 (2005) 95–102.
[10] V.I. Rizov, Non-linear indentation behavior of foam core sandwich composite materials – a 2D approach, Comput. Mater. Sci. 35 (2006) 107–115.
[11] C. Wang, H. Zhang, G. Shi, 3-D finite element simulation of impact damage of laminated plates using solid-shell interface elements, Appl. Mech. Mater. 130-132 (2012) 766–770.
[12] V.N. Burlayenko, T. Sadowski, A numerical study of the dynamic response of sandwich plates initially damaged by low-velocity impact, Comput. Mater. Sci. 52 (2012) 212–216.
[13] G. Goodmiller, S. TerMaath, Investigation of composite patch performance under low-velocity impact loading, in: 55th AIAA/ASME/ASCE/AHS/SC Structures, Structural Dynamics, and Materials Conference, National Harbor, Maryland, USA.
[14] N. Carrere, T. Vandellos, E. Martin, Multilevel analysis of delamination initiated near the edges of composite structures, in: 17th International Conference on Composite Materials (ICCM17), pp. 1–10. 27–31 July 2009, Edinburgh, UK.
[15] J.-S. Ahn, Y.-W. Kim, K.-S. Woo, Analysis of circular free edge effect in composite laminates by p-convergent global-local model, Int. J. Mech. Sci. 66 (2013) 149–155.
[16] T. Özben, N. Arslan, FEM analysis of laminated composite plate with rectangular hole and various elastic modulus under transverse loads, Appl. Math. Model. 34 (2010) 1746–1762.
[17] J.-S. Ahn, K.-S. Woo, D.-W. Lee, Delamination analysis of carbon fiber-reinforced peek using coarse mesh, Adv. Mater. Res. 538-541 (2012) 1624–1629.
[18] M. Hajikazemi, M. Sadr, A variational model for stress analysis in cracked laminates with arbitrary symmetric lay-up under general in-plane loading, Int. J. Solids Structures 51 (2014) 516–529.
[19] M. Hajikazemi, M. Sadr, Stiffness reduction of cracked general symmetric laminates using a variational approach, Int. J. Solids Structures 51 (2014) 1483–1493.
[20] E. Manoach, J. Warminski, A. Mitura, S. Samborski, Dynamics of a composite Timoshenko beam with delamination, Mech. Res. Commun. 46 (2012) 47–53.
[21] E. Manoach, J. Warminski, A. Mitura, S. Samborski, Dynamics of a laminated composite beam with delamination and inclusions, Eur. Phys. J. Special Topics 222 (2013) 1649–1664.
[22] E. Manoach, S. Samborski, A. Mitura, J. Warminski, Vibration based damage detection in composite beams under temperature variations using Poincaré maps, Int. J. Mech. Sci. 62 (2012) 120–132.
[23] A. Szekrényes, Coupled flexural-longitudinal vibration of delaminated composite beams with local stability analyis, J. Sound Vibration 333 (2014) 5141–5164.
[24] A. Szekrényes, A special case of parametrically excited systems: free vibration of delaminated composite beams, Eur. J. Mech. A/Solids 49 (2015) 82–105.
[25] H. Ovesy, A. Totounferoush, S. Ghannadpour, Dynamic buckling analysis of delaminated composite plates using semi-analytical finite strip method, J. Sound Vibrat. 343 (2015) 131–143.
[26] D.A. Hills, P.A. Kelly, D.N. Dai, A.M. Korsunsky, Solution of Crack Problems, The Distributed Dislocation Technique, Kluwer Academic Publishers, Dordrecht, Boston, London, 1996.
[27] V.E. Petrova, L. Marsavina, T. Sadowski, Revisit of compact mode II crack specimen: analysis and fracture interpretation, Theoret. Appl. Fract. Mech. 59 (2012) 41–48.
[28] V.E. Petrova, T. Sadowski, Theoretical analysis of mode II cracks in a compact shear specimen, Comput. Mater. Sci. 64 (2012) 248–252.
[29] S. Parvanova, Calculation of stress intensity factors based on force-displacement curve using element free Galerkin method, J. Theor. Appl. Mech. 42 (2012) 23–40. Sofia.
[30] D. Gardeazabal, Z. He, A. Kotousov, On influence of non-singular states on brittle fracture, Int. J. Fract. 185 (2014) 201–208.
[31] V. Rizov, Mixed-mode I/II fracture study of polymer composites using single edge notched bend specimens, Comput. Mater. Sci. 77 (2013) 1–6.
[32] B.D. Davidson, Encyclopedia of Aerospace Engineering, John Wiley & Sons, Ltd,
[33] M.F.S.F. De Moura, R.M. Guedes, L. Nicolais, Wiley Encyclopedia of Composites, Fracture: Interlaminar, John Wiley & Sons, Inc.
[34] M.A. Hamed, A. Nosier, G.H. Farrahi, Separation of delamination modes in composite beams with symmetric delaminations, Mater. Des. 27 (2006) 900–910.
[35] L. Sorensen, J. Botsis, T. Gmür, J. Cugnoni, Delamination detection and characterisation of bridging tractions using long FBG optical sensors, Compos. Part A – Appl. Sci. Manuf. 38 (2007) 2087–2096.
[36] M.M. Islam, R.K. Kapania, Delamination Growth using Cohesive Zone Model for Adhesive Bonding under Compression, Experimental and Applied Mechanics, 6, Springer, New York, 2011, pp. 527–536.
[37] M.M. Islam, R.K. Kapania, Global-local finite element analysis of adhesive joints and crack propagation, J. Aircraft 51 (2014) 310–319.
[38] S. Kim, J.S. Kim, H. Yoon, Experimental and numerical investigations of mode I delamination behaviors of woven fabric composites with carbon, Kevlar and their hybrid fibers, Int. J. Precis. Eng. Manuf. 12 (2011) 321–329.
[39] L. Peng, J. Zhang, L. Zhao, R. Bao, H. Yang, B. Fei, Mode I delamination growth of multidirectional composite laminates under fatigue loading, J. Compos. Mater. 45 (2011) 1077–1090.

Please cite this article as: A. Szekrényes, Semi-layerwise analysis of laminated plates with nonsingular delamination—The theorem of autocontinuity, Applied Mathematical Modelling (2015), http://dx.doi.org/10.1016/j.apm.2015.06.037

UNCORRECTED PROOF

[40] J. Jumel, M.K. Budzik, M.E.R. Shanahan, Beam on elastic foundation with anticlastic curvature: application to analysis of mode I fracture tests, Eng. Fract. Mech. 78 (2011) 3253–3269.
[41] N.B. Salem, M.K. Budzik, J. Jumel, M.E.R. Shanahan, F. Lavelle, Investigation of the crack front process zone in the double cantilever beam test with backface strain monitoring technique, Eng. Fract. Mech. 98 (2013) 272–283.
[42] I. de Baere, S. Jacques, W.V. Paepegem, J. Degrieck, Study of the mode I and mode II interlaminar behaviour of a carbon fabric reinforced thermoplastic, Polymer Testing 31 (2012) 322–332.
[43] J.D. Gracia, A. Boyano, A. Arrese, F. Mujika, A new approach for determining the R-curve in DCB tests without optical measurements, Eng. Fract. Mech. 135 (2015) 274–285.
[44] H. Yoshihara, A. Satoh, Shear and crack tip deformation correction for the double cantilever beam and three-point end-notched flexure specimens for mode I and mode II fracture toughness measurement of wood, Eng. Fract. Mech. 76 (2009) 335–346.
[45] A. Arrese, N. Carbajal, G. Vargas, F. Mujika, A new method for determining mode II R-curve by the end-notched flexure test, Eng. Fract. Mech. 77 (2010) 51–70.
[46] A. Argüelles, J.V. na, A.F. Canteli, J. Bonhomme, Influence of resin type on the delamination behavior of carbon fiber reinforced composites under mode-II loading, Int. J. Damage Mech. 20 (2011) 963–977.
[47] V. Rizov, A.S. Mladensky, Analysis of mode II crack in bilayered composite beam, J. Theoret. Appl. Mech. 42 (2012) 67–78.
[48] M.F.S.F. de Moura, R.D.S.G. Campilho, J.P.M. Gonçalves, Pure mode II fracture characterization of composite bonded joints, Int. J. Solids Struct. 46 (2009) 1589–1595. (Cited by 48).
[49] M.F.S.F. de Moura, R. Fernandes, F.G.A. Silva, N. Dourado, Mode II fracture characterization of a hybrid cork/carbon-epoxy laminate, Compos. Part B: Eng. 76 (2015) 44–51.
[50] V. Rizov, Y. Shindo, K. Horiguchi, F. Narita, Mode III interlaminar fracture behaviour of glass fiber reinforced polymer woven laminates at 293 to 4 k, Appl. Compos. Mater. 13 (2006) 287–304.
[51] A. Szekrényes, Improved analysis of the modified split-cantilever beam for mode III fracture, Int. J. Mech. Sci. 51 (2009) 682–693.
[52] H. Yoshihara, Examination of the 4-ENF test for measuring the mode III R-curve of wood, Eng. Fract. Mech. 73 (2006) 42–63.
[53] R.M. Marat-Mendes, M.M. Freitas, Characterisation of the edge crack torsion (ECT) test for the measurement of the mode III interlaminar fracture toughness, Eng. Fract. Mech. 76 (2009) 2799–2809.
[54] H. Suemasu, Y. Tanikado, Delamination propagation behavior and the fracture toughness of composite laminates under shear fracture mode, in: 27th Annual Technical Conference of the American Society for Composites 2012, Held Jointly with 15th Joint US–Japan Conference on Composite Materials and ASTM-D30 Meeting, pp. 367–379.
[55] A. Szekrényes, The influence of crack length and delamination width on the mode-III energy release rate of laminated composites, J. Compos. Mater. 45 (2011) 279–294.
[56] A.L. Johnston, B.D. Davidson, K.K. Simon, Evaluation of new test methods for the determination of G_{IIIc} of laminated polymeric composites, in: 27th Annual Technical Conference of the American Society for Composites 2012, Held Jointly with 15th Joint US–Japan Conference on Composite Materials and ASTM-D30 Meeting, pp. 120–139.
[57] F.A. Mehrabadi, M. Khosravan, Mode III interlaminar fracture in woven glass/epoxy composite laminates, World Acad. Sci. Eng. Technol. 73 (2013) 479–483.
[58] A. Johnston, B. Davidson, K. Simon, Assessment of split-beam-type tests for mode III delamination toughness determination, Int. J. Fract. 185 (2014) 31–48.
[59] A. Johnston, B. Davidson, Intrinsic coupling of near-tip matrix crack formation to mode III delamination advance in laminated polymeric matrix composites, Int. J. Solids Struct. 51 (2014) 2360–2369.
[60] J. Rodríguez-González, A. May-Pat, F. Avilés, A beam specimen to measure the face/core fracture toughness of sandwich materials under a tearing loading mode, Int. J. Mech. Sci. 79 (2014) 84–94.
[61] M.R. Khoshravan, M. Moslemi, Investigation on mode III interlaminar fracture of glass/epoxy laminates using a modified split cantilever beam test, Eng. Fract. Mech. 127 (2014) 267–279.
[62] A. López-Menéndez, J.V. na, A. Argüelles, J. Bonhomme, V. Mollón, M. Lozano, A new methodology for testing composite materials in mode III of fracture, 16th European Conference on Composite Materials, ECCM 2014, June 22–26, Sevilla, Spain.
[63] G. Cricrì, M. Perrella, S. Sessa, N. Valoroso, A novel fixture for measuring mode III toughness of bonded assemblies, Eng. Fract. Mech. 138 (2015) 1–18.
[64] M. Nikbakht, N. Choupani, Fracture toughness characterization of carbon-epoxy composite using Arcan specimen, World Acad. Sci. Eng. Technol. 41 (2008) 738–744.
[65] S. Bennati, M. Colleluori, D. Corigliano, P.S. Valvo, An enhanced beam-theory model of the asymmetric double cantilever beam (ADCB) test for composite laminates, Compos. Sci. Technol. 69 (2009) 1735–1745.
[66] M. Kenane, S. Benmedakhene, Z. Azari, Fracture and fatigue study of unidirectional glass/epoxy laminate under different mode of loading, Fatigue Fract. Eng. Mater. Struct. 33 (2010) 285–293.
[67] B. Davidson, A. Bansal, Q. Bing, X. Sun, Geometrically nonlinear determination of energy release rate and mode ratio in single leg bending tests, J. Reinforced Plastics Compos. 28 (2009) 1881–1901.
[68] J. Jumel, M.K. Budzik, M.E.R. Shanahan, Process zone in the single cantilever beam under transverse loading. Part I. Theoretical analysis, Theoretical Appl. Fract. Mech. 56 (2011) 7–12.
[69] L.F.M.d. Silva, V.H.C. Estevez, F.J.P. Chavez, Fracture toughness of a structural adhesive under mixed mode loadings, Materialwissen. Werkstofftech. 42 (2011) 460–470.
[70] M.V. Fernández, M.F.S.F. Moura, L.F.M. da Silva, A.T. Marques, Mixed-mode fatigue/fracture characterization of composite bonded joints using the single-leg bending test, Compos. Part A: Appl. Sci. Manuf. 44 (2013) 63–69.
[71] S. Wang, C.M. Harvey, Mixed mode partition theories for one dimensional fracture, Eng. Fract. Mech. 79 (2012) 329–352.
[72] S. Bennati, P. Fisicaro, P.S. Valvo, An enhanced beam-theory model of the mixed-mode bending (MMB) test. Part I. Literature review and mechanical model, Meccanica 48 (2013) 443–462.
[73] S. Bennati, P. Fisicaro, P.S. Valvo, An enhanced beam-theory model of the mixed-mode bending (MMB) test – Part II: applications and results, Meccanica 48 (2013) 465–484.
[74] A. Mladensky, V. Rizov, Non-linear fracture study of single cantilever beam specimen, ZAMM – Zeitschrift für Angewandte Mathematik und Mechanik (2014) 1–13, doi:10.1002/zamm.201400104.
[75] P. Liu, J. Yang, B. Wang, Z. Zhou, J. Zheng, A study on the intralaminar damage and interlaminar delamination of carbon fiber composite laminates under three-point bending using acoustic emission, J. Failure Anal. Prev. 15 (2015) 101–121.
[76] G. Charalambous, G. Allegri, J.K. Lander, S.R. Hallett, A cut-ply specimen for the mixed-mode fracture toughness and fatigue characterisation of FRPs, Compos. Part A: Appl. Sci. Manuf. 74 (2015) 77–87.
[77] A. Szekrényes, Interlaminar fracture analysis in the G_I-G_{III} plane using prestressed transparent composite beams, Compos. Part A – Appl. Sci. Manuf. 40 (2009) 1621–1631.
[78] M. Miura, Y. Shindo, T. Takeda, F. Narita, Mixed-mode I/III fatigue delamination growth in woven glass/epoxy composite laminates at cryogenic temperatures, J. Compos. Mater. 48 (2014) 1251–1259.
[79] A. Szekrényes, Delamination fracture analysis in the G_{II}-G_{III} plane using prestressed composite beams, Int. J. Solids Struct. 44 (2007) 3359–3378.
[80] H. Suemasu, A. Kondo, K. Gozu, Y. Aoki, Novel test method for mixed mode II and III interlaminar fracture toughness, Adv. Compos. Mater. 19 (2010) 349–361.
[81] S.L. Ho, A.A.O. Tay, A numerical analysis of penny-shaped delaminations in an encapsulated silicon module, IEEE, in: IEEE 61st Electronic Components and Technology Conference (ECTC), 2011, pp. 1115–1121

UNCORRECTED PROOF

Please cite this article as: A. Szekrényes, Semi-layerwise analysis of laminated plates with nonsingular delamination—The theorem of autocontinuity, Applied Mathematical Modelling (2015), http://dx.doi.org/10.1016/j.apm.2015.06.037

[82] A. Kondo, Y. Sato, H. Suemasu, Y. Aoki, Fracture resistance of carbon/epoxy composite laminates under mixed-mode II and III failure and its dependence on fracture morphology, Adv. Compos. Mater. 20 (2011) 405–418.
[83] A. Kondo, Y. Sato, H. Suemasu, K. Gouzu, Y. Aoki, Characterization of fracture resistance of carbon/epoxy composite laminates during mixed-mode II and III stable damage propagation, J. Jpn. Soc. Compos. Mater. 36 (2010) 179–188.
[84] M. Nikbakht, N. Choupani, S.R. Hosseini, 2D and 3D interlaminar fracture assessment under mixed-mode loading conditions, Mater. Sci. Eng. A 516 (2010) 162–168.
[85] A. Szekrényes, Interlaminar fracture analysis in the G_{II}-G_{III} plane using prestressed transparent composite beams, Compos. Part A – Appl. Sci. Manuf. 43 (2012) 95–103.
[86] M. Miura, Y. Shindo, T. Takeda, F. Narita, Interlaminar fracture characterization of woven glass/epoxy composites under mixed-mode II/III loading conditions at cryogenic temperatures, Eng. Fract. Mech. 96 (2012) 615–625.
[87] T. Takeda, M. Miura, Y. Shindo, F.F. Narita, Fatigue delamination growth in woven glass/epoxy composite laminates under mixed-mode II/III loading conditions at cryogenic temperatures, Cryogenics 58 (2013) 55–61.
[88] F.A. Mehrabadi, Analysis of pure mode III and mixed mode (III+ II) interlaminar crack growth in polymeric woven fabrics, Mater. Des. 44 (2013) 429–437.
[89] A.S. Mladensky, V. Rizov, Analysis of mixed mode II/III crack in bilayered composite beam, J. Theoret. Appl. Mech. 42 (2013) 41–52.
[90] B.D. Davidson, F.O. Sediles, K.D. Humphrey, A shear-torsion-bending test for mixed-mode I-II-III delamination toughness determination, in: 25th Technical Conference of the American Society for Composites and 14th US-Japan Conference on Composite Materials, 20–22 September 2010, Dayton, Ohio, USA, volume 2, pp. 1001–1020.
[91] A. Szekrényes, Interlaminar fracture analysis in the G_I-G_{II}-G_{III} space using prestressed transparent composite beams, J. Reinforced Plastics Compos. 30 (2011) 1655–1669.
[92] B.D. Davidson, F.O. Sediles, Mixed-modeI-II-III delamination toughness determination via a shear-torsion-bending test, Compos. Part A: Appl. Sci. Manufacturing 42 (2011) 589–603.
[93] J.N. Reddy, Mechanics of Laminated Composite Plates and Shells – Theory and Analysis, CRC Press, Boca Raton, London, New York, Washington, D.C., 2004.
[94] L.P. Kollár, G.S. Springer, Mechanics of Composite Structures, Cambridge University Press, Cambridge, New York, Melbourne, Madrid, Cape Town, Singapore, São Paolo, 2003.
[95] H. Hajheidari, H.R. Mirdamadi, Frequency-dependent vibration analysis of symmetric cross-ply laminated plate of Levy-type by spectral element and finite strip procedures, Appl. Math. Model. 37 (2013) 7193–7205.
[96] V. Radosavljević, M. Dražić, Exact solution for buckling of FCFC stepped rectangular plates, Appl. Math. Model. 34 (2010) 3841–3849.
[97] A. Assie, A. Kabeel, F. Mahmoud, Optimum design of laminated composite plates under dynamic excitation, Appl. Math. Model. 36 (2012) 668–682.
[98] J. Petrolito, Vibration and stability analysis of thick orthotropic plates using hybrid-Trefftz elements, Appl. Math. Model. 38 (2014) 5858–5869.
[99] M. Endo, Study on an alternative deformation concept for the Timoshenko beam and Mindlin plate models, Int. J. Eng. Sci. 87 (2015) 32–46.
[100] M. Endo, N. Kimura, An alternative formulation of the boundary value problem for the Timoshenko beam and Mindlin plate, J. Sound Vibrat. 301 (2007) 355–373.
[101] H. Ovesy, M. Naghinejad, M. Kharazi, Delamination growth speed analysis in a compressed composite laminate based on first-order shear deformation theory, J. Compos. Mater. (2015).
[102] A.A. Khdeir, J.N. Reddy, Free vibrations of laminated composite plates using second-order shear deformation theory, Comput. Struct. 71 (1999) 617–626.
[103] A. Shahrjerdi, F. Mustapha, M. Bayat, D.L.A. Majid, Free vibration analysis of solar functionally graded plates with temperature-dependent material properties using second order shear deformation theory, J. Mech. Sci. Technol. 25 (2011) 1–15.
[104] A. Szekrényes, Interface fracture in orthotropic composite plates using second-order shear deformation theory, Int. J. Damage Mech. 22 (2013) 1161–1185.
[105] M. Izadi, M. Tahani, Analysis of interlaminar stresses in general cross-ply laminates with distributed piezoelectric actuators, Compos. Struct. (2010) 757–768.
[106] A. Szekrényes, Antiplane–inplane shear mode delamination between two second-order shear deformable composite plates, Math. Mech. Solids (2015) 1–24, doi:10.1177/1081286515581871.
[107] M. Talha, B. Singh, Static response and free vibration analysis of FGM plates using higher order shear deformation theory, Appl. Math. Model. 34 (2010) 3991–4011.
[108] S.K. Panda, B.N. Singh, Large amplitude free vibration analysis of thermally post-buckled composite doubly curved panel using nonlinear FEM, Finite Elements Anal. Des. 47 (2011) 378–386.
[109] V.K. Singh, S.K. Panda, Nonlinear free vibration analysis of single/doubly curved composite shallow shell panels, Thin-Walled Struct. 85 (2014). 431–349.
[110] S.K. Panda, B.N. Singh, Nonlinear free vibration of spherical shell panel using higher order shear deformation theory – a finite element approach, Int. J. Pressure Vessels Piping 86 (2009) 373–383.
[111] A. Szekrényes, Stress and fracture analysis in delaminated orthotropic composite plates using third-order shear deformation theory, Appl. Math. Model. 38 (2014) 3897–3916.
[112] C.H. Thai, L.V. Tran, D.T. Tran, T. Nguyen-Thoi, H. Nguyen-Xuan, Analysis of laminated composite plates using higher-order shear deformation plate theory and node-based smoothed discrete shear gap method, Appl. Math. Model. 36 (2012) 5657–5677.
[113] A.S. Oktem, V. Alankaya, C.G. Soares, Boundary-discontinuous Fourier analysis of simply supported cross-ply plates, Appl. Math. Model. 37 (2013) 1378–1389.
[114] A. Szekrényes, Bending solution of third-order orthotropic Reddy plates with asymmetric interfacial crack, Int. J. Solids Structures 51 (2014) 2598–2619.
[115] M.G. Taj, A. Chakrabarti, A.H. Sheikh, Analysis of functionally graded plates using higher order shear deformation theory, Appl. Math. Model. 37 (2013) 8484–8494.
[116] A.J.M. Ferreira, C.M.C. Roque, E. Carrera, M. Cinefra, O. Polit, Two higher order zig-zag theories for the accurate analysis of bending, vibration and buckling response of laminated plates by radial basis functions collocation and a unified formulation, J. Compos. Mater. 45 (2011) 2523–2536.
[117] P. Malekzadeh, A. Afsari, P. Zahedinejad, R. Bahadori, Three-dimensional layerwise-finite element free vibration analysis of thick laminated annular plates on elastic foundation, Appl. Math. Model. 34 (2010) 776–790.
[118] R. Sahoo, B. Singh, A new trigonometric zigzag theory for static analysis of laminated composite and sandwich plates, Aerosp. Sci. Technol. 35 (2014) 15–28.
[119] R. Sahoo, B. Singh, A new trigonometric zigzag theory for buckling and free vibration analysis of laminated composite and sandwich plates, Compos. Structures 117 (2014) 316–332.
[120] R. Sahoo, B. Singh, A new inverse hyperbolic zigzag theory for the static analysis of laminated composite and sandwich plates, Compos. Struct. 105 (2013) 385–397.
[121] F.A. Mehrabadi, M. Khoshravan, Mode III interlaminar fracture and damage characterization in woven fabric-reinforced glass/epoxy composite laminates, J. Compos. Mater. 47 (2013) 1583–1592.
[122] F.A. Mehrabadi, The use of ECT and 6PBP tests to evaluate fracture behavior of adhesively bonded steel/epoxy joints under mode-III and mixed mode III/II, Appl. Adhesion Sci. 2 (2014) 1–15.
[123] A. Szekrényes, Analysis of classical and first-order shear deformable cracked orthotropic plates, J. Compos. Mater. 48 (2014a) 1441–1457.
[124] A. Szekrényes, Application of Reddy's third-order theory to delaminated orthotropic composite plates, Eur. J. Mech. A/Solids 43 (2014b) 9–24.
[125] A. Szekrényes, The system of exact kinematic conditions and application to delaminated first-order shear deformable composite plates, Int. J. Mech. Sci. 77 (2013) 17–29.
[126] A. Szekrényes, Antiplane-inplane shear mode delamination between two second-order shear deformable composite plates, Math. Mech. Solids (2014). (in press).
[127] N. Saeedi, K. Sab, J.-F. Caron, Delaminated multilayered plates under uniaxial extension. Part I. Analytical analysis using a layerwise stress approach, Int. J. Solids Struct. 49 (2012) 3711–3726.

Please cite this article as: A. Szekrényes, Semi-layerwise analysis of laminated plates with nonsingular delamination—The theorem of autocontinuity, Applied Mathematical Modelling (2015), http://dx.doi.org/10.1016/j.apm.2015.06.037

UNCORRECTED PROOF

[128] N. Saeedi, K. Sab, J.-F. Caron, Delaminated multilayered plates under uniaxial extension. Part II. Efficient layerwise mesh strategy for the prediction of delamination onset, Int. J. Solids Structures 49 (2012) 3727–3740.
[129] N. Saeedi, K. Sab, J.-F. Caron, Cylindrical bending of multilayered plates with multi-delamination via a layerwise stress approach, Comp. Struct. 95 (2013) 728–739.
[130] N. Saeedi, K. Sab, J.-F. Caron, Stress analysis of long multilayered plates subjected to invariant loading: Analytical solutions by a layerwise stress model, Compos. Struct. 100 (2013) 307–322.
[131] A. Kotousov, P. Lazzarin, F. Berto, L. Pook, Three-dimensional stress states at crack tip induced by shear and anti-plane loading, Eng. Fract. Mech. 108 (2013) 65–74.
[132] A. Kotousov, F. Berto, P. Lazzarin, F. Pegorin, Three dimensional finite element mixed fracture mode under anti-plane loading of a crack, Theoret. Appl. Fract. Mech. 62 (2012) 26–33.
[133] N. Baddour, Second order shear deformation theory (SSDT) for free vibration analyis on a functionally graded quadrangle plate, in: A. Shahrjerdi and F. Mustapha (Eds.), Recent Advances in Vibration Analysis. Intech pp. 60–78.
[134] P.C. Chou, N.J. Pagano, Elasticity – Tensor, Dyadic, and Engineering Approaches, D. Van Nostrand Company, Inc., Princeton, New Jersey, Toronto, London, 1967.
[135] S. Hosseini-Hashemi, M. Fadaee, H.R.D. Taher, Exact solutions for free flexural vibration of Lévy-type rectangular thick plates via third-order shear deformation, Appl. Math. Model. 35 (2011) 708–727.
[136] H.-T. Thai, S.-E. Kim, Lévy-type solution for free vibration analysis of orthotropic plates based on two variable refined plate theory, Appl. Math. Model. 36 (2012) 3870–3882.
[137] M. Bodaghi, A.R. Saidi, Lévy-type solution for buckling analysis of thick functionally graded rectangular plates based on the higher-order, Appl. Math. Model. 34 (2010) 3659–3673.
[138] Y. Jianqiao, Laminated Composite Plates and Shells – 3D Modelling, Springer, London, Berlin, Heidelberg, New York, Hong Kong, Milan, Paris, Tokyo, 2003.
[139] J. Bonhomme, A. Argüelles, M.A. Castrillo, J. Vina, Computational models for mode I composite fracture failure: the virtual crack closure technique versus the two-step extension method, Meccanica 45 (2010) 297304.
[140] H.-T. Thai, T.P. Vo, A new sinusoidal shear deformation theory for bending, buckling, and vibration of functionally graded plates, Appl. Math. Model. 37 (2013) 3269–3281.
[141] G. Shi, A new simple third-order shear deformation theory of plates, Int. J. Solids Struct. 44 (2007) 4399–4417.
[142] A. Alibeigloo, A.P. Zanoosi, Static analysis of rectangular nano-plate using three-dimensional theory of elasticity, Appl. Math. Model. 37 (2013) 7016–7026.
[143] H.-T. Thai, D.-H. Choi, Analytical solutions of refined plate theory for bending, buckling and vibration analyses of thick plates, Appl. Math. Model. 37 (2013) 8310–8323.
[144] J. Mantari, A. Oktem, C.G. Soares, A new trigonometric shear deformation theory for isotropic, laminated composite and sandwich plates, Int. J. Solids Struct. 49 (2012) 43–53.
[145] R. Sahoo, B. Singh, A new shear deformation theory for the static analysis of laminated composite and sandwich plates, Int. J. Mech. Sci. 75 (2013) 324–336.

UNCORRECTED PROOF

Please cite this article as: A. Szekrényes, Semi-layerwise analysis of laminated plates with nonsingular delamination—The theorem of autocontinuity, Applied Mathematical Modelling (2015), http://dx.doi.org/10.1016/j.apm.2015.06.037